NOVA SCHOOL OF SCIENCE & TECHNOLOGY

DEPARTMENT OF Materials Science

Daniel Pereira Camilo

BSc in Micro and Nanotechnologies Engineering

Air Processed Stable Wide-Bandgap $MAPbBr_3$ Perovskite Solar Cells

MASTER IN Micro and Nanotechnologies Engineering

NOVA University Lisbon

October 2023

NOVA SCHOOL OF SCIENCE & TECHNOLOGY

DEPARTMENT OF
Materials Science

Air Processed Stable Wide-Bandgap $MAPbBr_3$ Perovskite Solar Cells

Daniel Pereira Camilo

BSc in Micro and Nanotechnologies Engineering

Adviser: Dr. Ugur Deneb Menda
Senior Researcher, School of science and Technology-
NOVA University Lisbon

Co-advisers: Dr. Manuel J. Mendes
Assistant Professor, School of science and Technology-
NOVA University Lisbon

Examination Committee:

Chair: Dr. Hugo Manuel Brito Águas,
Full Professor, FCT-NOVA

Rapporteurs: Dr. Iñigo Gonzalez Ramiro,
Senior Researcher, Instituto de Energía Solar
Universidad Politécnica de Madrid

Adviser: Dr. Ugur Deneb Menda ,
Senior Researcher, School of science and Technology-
NOVA University Lisbon

MASTER IN MICRO AND NANOTECHNOLOGIES ENGINEERING

NOVA University Lisbon
October 2023

Air Processed Stable Wide-Bandgap MAPbBr3 Perovskite Solar Cells

This document was created with Microsoft Word text processor and the NOVAthesis Word template [67].

ACKNOWLEDGMENTS

Quero começar por agradecer aos meus orientadores, a Dra. Deneb Menda e Prof. Manuel Mendes, por me terem dado a oportunidade de trabalhar numa área de extrema importância, na qual tenho bastante interesse. Agradeço também por me terem auxiliado aos longo destes meses e pela partilha do seu conhecimento.

De seguida, agradeço ao CENIMAT e UNINOVA por disponibilizarem os seus laboratórios equipados com todos os equipamentos necessários para a realização desta dissertação.

Quero agradecer a todos os meus amigos, quer aos de longa data, quer àqueles que fiz durante o meu percurso académico que me acompanharam durante os últimos 5 anos, em especial a todos aqueles com quem tive a oportunidade de partilhar a excelente Pizza da Cantina. O vosso apoio foi essencial para completar esta grande etapa.

Finalmente, e não menos importante, quero agradecer à minha família, em especial aos meus pais, irmã, avós e ao Benny por me terem apoiado durante todo o meu percurso. Agradeço por terem estado ao meu lado nos bons e nos maus momentos, pelas palavras de encorajamento, pela compreensão e pela paciência. Do fundo do meu coração, um grande obrigado, pois sem vocês nada disto seria possível!

Obrigado a todos!

“You cannot teach a man anything; you can only help him discover it in himself.” (Galileo).

ABSTRACT

The high sensitivity of perovskite solar cells (PSCs) prevents them from revolutionising the renewable energy landscape. With this in mind, this thesis aims to manufacture PSCs with greater stability, primarily focusing on optimising the active layer. To achieve this goal, the study was focused on $CH_3NH_3PbBr_3$, a perovskite with a wide-bandgap of 2.30 eV, known for its superior stability compared to more extensively researched organohalide perovskites. Its deposition is carried out using the spin-coating technique under ambient air conditions, which makes the process more challenging, due to its sensitivity to environmental conditions such as temperature and relative humidity. In order to promote the enhancement of the stability of PSCs, the addition of quantum dots (QDs) at different concentrations in the perovskite matrix was investigated. To support this research, the synthesised thin films were characterised using SEM, XRD, PL and UV-Vis spectrophotometry. The optoelectronic performance of the devices was also analysed whilst they were stored in vacuum and in ambient air, to assess their stability in different environments.

The introduction of QDs was successful, especially at a concentration of 2.00 mg/mL, as it reduced the degradation rate of the devices. After 1320 hours in vacuum, cells manufactured with QDs increased their power conversion efficiency (PCE) from 2.03 % to 2.39 %, an increase of 18 %. In contrast, in pristine cells a 41.9 % decrease was observed, from 1.24 % to 0.72 %. When exposed to ambient air, the pristine devices ceased to operate entirely, whilst devices with QDs maintained a PCE 12 % higher than the initial value, this is, 2.28 %.

Keywords: Photovoltaics, Wide-bandgap perovskite solar cells, PbS quantum dots, Air-processing, Enhanced stability

RESUMO

A alta sensibilidade das células solares de *perovskite* (PSCs) previne-as de revolucionarem o panorama das energias renováveis. Posto isto, esta tese tem como objetivo a fabricação de PSCs com maior estabilidade, focando maioritariamente na otimização da camada ativa. Para tal, recorreu-se ao estudo de $CH_3NH_3PbBr_3$, uma *perovskite* com *wide-bandgap* de 2.30 eV, com estabilidade superior relativamente às *organohalide perovskites* mais investigadas. A sua deposição é realizada através da técnica de *spin-coating* em condições de ar ambiente, algo que torna o processo mais desafiador, dada a sua sensibilidade à temperatura e humidade relativa. De modo a promover o maior aumento da estabilidade das PSCs, foi estudada a adição de *quantum dots* (QDs) em diferentes concentrações na matriz da *perovskite*. Para apoiar esta pesquisa, os filmes finos sintetizados foram caracterizados por SEM, XRD e espetrofotometria PL e UV-Vis. O desempenho optoelectrónico dos dispositivos foi também analisado enquanto estes se encontravam armazenados em vácuo e em ar ambiente, de modo a averiguar a sua estabilidade em diferentes meios.

A introdução dos QDs foi um sucesso, em especial com uma concentração de 2.00 mg/mL, dado que permitiu reduzir o ritmo de degradação dos dispositivos. Depois de 1320 h em vácuo, células fabricadas com QDs aumentaram a sua eficiência de conversão de potência (PCE) de 2.03 % para 2.39 %, um aumento de 18 %. Por outro lado, nas células pristinas observou-se um decréscimo em 41.9 %, de1.24 % para 0.72 %. Quando expostos ao ar ambiente, os dispositivos pristinos deixaram totalmente de operar, enquanto os dispositivos com QDs apresentaram uma PCE 12 % superior à inicial, isto é, 2.28 %.

Palavas chave: Fotovoltaico, Células solares de *wide-bandgap* perovskite, Quantum dots de PbS, Processamento em ar ambiente, Estabilidade melhorada

CONTENTS

LIST OF FIGURES

LIST OF TABLES

ACRONYMS

AFM	Atomic force microscopy
AMX_3	Perovskite structure (generic formula)
c-TiO_2	Compact titanium dioxide
DMF	Dimethylformamide
DMSO	Dimethyl sulfoxide
EDX	Energy dispersed X-ray spectroscopy
ETL	Electron transport layer
FF	Fill factor
FWHM	Full width at half maximum
GB	Glovebox
HTL	Hole transport layer
IBSCs	Intermediate band solar cells
ITO	Indium tin oxide
LEDs	Light-emitting diodes
m-TiO_2	Mesoporous titanium oxide
MA^+	Methyl ammonium
MABr	Methylammonium bromide
$MAPbBr_3$	Methylammonium lead bromide
$MAPbI_3$	Methylammonium lead iodide
PbS	Lead sulphide
$PbBr_2$	Lead bromide
PbI_2	Lead iodide
PCE	Power conversion efficiency
PL	Photoluminescence
PSCs	Perovskite solar cells

PV	Photovoltaic
QDs	Colloidal quantum dots
RH	Relative humidity
SEM	Scanning electron microscopy
SnO_2	Tin dioxide
Spiro-MeOTAD	2,2',7,7'-Tetrakis[N,N-di(4-methoxyphenyl)amino]-9,9'-spirobifluorene
TCO	Transparent conducting oxide
UV-Vis	Ultraviolet-visible spectrophotometry
XRD	X-ray diffraction

SYMBOLS

nm	Nanometre
µm	Micrometre
mm	Millimetre
cm	Centimetre
mg	Milligram
µL	Microlitre
mL	Millilitre
M	Molar concentration
s	Second
min	Minute
h	Hour
rpm	Rotations per minute
V	Volts
mA	Milliampere
Ω	Ohm
eV	Electron Volt
λ	Wavelength
sq	Square
°C	Degrees Celsius
$\mathbf{E_G}$	Bandgap energy
J_{SC}	Short-circuit current density
V_{OC}	Open circuit voltage

MOTIVATION AND OBJECTIVES

Climate change is causing increasingly frequent and severe consequences, such as extreme weather events and global temperature rise, ultimately resulting in unprecedented ecological disruptions. For this matter, the pursuit of sustainable, clean, and renewable energy sources has been more critical than ever. Photovoltaic systems, being able to capture the limitless energy from the sun, can produce clean electricity, therefore playing a crucial role in tackling the effects of climate change.

Silicon-based solar cells currently dominate the solar energy market, making up approximately 95% of the global photovoltaic market (2023).[1] A major reason for its widespread use is the abundance of silicon, the primary raw material, which is the second most abundant element on Earth's crust. However, the production of silicon-based solar cells involves the use of vacuum systems and high temperature procedures that require great amounts of energy. For these reasons, new materials and technologies are sought to further enhance the sustainability of PV systems.

Thin films have emerged as an alternative technology to the traditional silicon-based solar cells. One of the most promising technologies in this field are perovskites solar cells (PSCs). Given their excellent properties, perovskites have been intensively studied over the last years, rapidly transforming the solar energy landscape. Their remarkable optoelectronic properties have led to significant efficiency enhancements, being the current power conversion efficiency record for single junction PSCs 26.1 %.[2] Not only that, but perovskites can also be integrated into tandem systems, in which when coupled with silicon solar cells allow to complement the traditional technology, achieving a current maximum power conversion efficiency (PCE) of 33.7 %.[2]

Nevertheless, the majority of the research has been mostly aimed on increasing the PSCs' PCE, so that they can compete with conventional silicon solar cells. This left another important subject unattended, PSCs' stability. Perovskites are extremely sensitive to environmental factors, such as moisture, oxygen, UV radiation and heat. This sensitivity presents a significant challenge for commercialisation, since prolonged exposure to these elements leads to rapid degradation, compromising, consequently, their long-term stability.[3], [4]

Therefore, the objective of this thesis, given the great potential of PSCs, is to study, and try to enhance their long-term stability, so that this technology can enter the photovoltaic market and revolutionise it. To achieve this goal, a different and more stable perovskite material ($MAPbBr_3$) with a wide-bandgap, of 2.30 eV, to be used in several applications that requires higher voltage outputs such as water splitting, tandem devices with other perovskites or other PV technologies, and great potential with Intermediate band solar cells (IBSCs), is used instead of the most common one ($MAPbI_3$), as the active layer for solar cells. Two different deposition approaches to deposit the absorber layer, one-step and two-step methods, are also studied. Additionally, an additive, 4-tert-buthylpyridine, is added to the perovskite matrix in order to try to increase the PCE of PSCs. Moreover, PbS-QDs, are incorporated into the perovskite matrix, since it has been demonstrated that, in small concentrations, are able to increase the stability of perovskite devices.

1

INTRODUCTION

1.1 Perovskite Solar Cells

In the previous years, hybrid organic-inorganic halide materials have been widely researched in photovoltaics because of their great optoelectronic properties.[5] These materials are characterised for having a crystal structure of perovskite, ABX_3, where A is a large cation, usually organic, like methylammonium (MA^+, $CH_3NH_3^+$) or formamidinium (FA^+, $NH_2CHNH_2^+$), B is also a cation but of smaller size, being lead (Pb) the most used element, although tin (Sn) has also been used, and X is a halogen anion, being iodide, bromide and chloride (I^-, Br^-, and Cl^-, respectively) the most used ones. Therefore, thin film solar cells composed by these materials are denominated perovskite solar cells (PSCs). PSCs follow, usually, a n-i-p structure of the following layers: glass that acts as the substrate; a transparent conducting oxide (TCO); an electron transporting layer (ETL); the absorber, a perovskite material; a hole transporting layer (HTL); and a metallic back contact, as seen in Figure 1.[6]

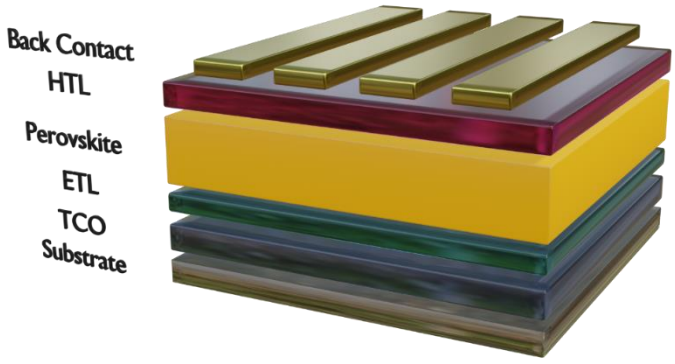

Figure 1. Perovskite solar cell n-i-p structure (not to scale)

The research of PSCs was first reported in 2009, with cells having a power conversion efficiency (PCE) of 3.8%, and, since then, many other studies have been published, resulting in a rapid improvement in efficiency in the following years.[6], [7] Currently, the record efficiency for single junction PSCs is 26.1 %, and for tandem solar cells, when coupled with silicon solar cells, the efficiency is 33.7 %.[2]

Perovskite materials have great properties that make them interesting to study. Some of these properties are high absorption coefficients, long carrier diffusion lengths and high charge carrier mobility, which ultimately, when in solar cells, allow for excellent performances, enabling high PCE values.[8] However, these are common requirements for all solar cells technologies. What distinguishes it from silicon solar cells is its low temperature processing, and easy and low-cost production. Additionally, depending on what halogen

element one chooses to use, perovskites' bandgap can be precisely tuned, ranging from 1.30 eV up to wide-bandgap values of 2.40 eV, allowing it to capture radiation from specific parts of the solar spectrum. For instance, by replacing the halogen material in $MAPb(I_{1-x}Br_x)_3$, I ions for Br ions, the bandgap is tuned from 1.50 eV to 2.30 eV.[9] Studies concerning record breaking efficiencies use mostly low-bandgap perovskites so that a wider range of the solar spectrum is absorbed, and, for this reason, perovskite containing iodine are used for this aim.

1.2 Wide-bandgap Perovskite Materials

Wide-bandgap perovskites, contrary to low-bandgap solar cells, do not cover as much of the solar spectrum. Nevertheless, it does not mean that wide-bandgap perovskites are not investigated. Such materials can be incorporated as the top layer when coupled with silicon or CIGS solar cells to fabricate double-junction tandem systems. For perovskites with really high bandgap energy values, for instance $MAPbBr_3$, triple-junction tandem solar cells can also be fabricated in a perovskite-perovskite-silicon tandem system that allows for greater PCE values.[10] Moreover, wide-bandgap perovskites can also be applied to fabricate solar water splitting and CO_2 reduction devices, since they can supply high voltages which are required for such applications.[11]

Another application for wide-bandgap perovskites is the fabrication of intermediate band solar cells (IBSC).[12] In IBSC, an intermediate band is introduced, for instance with the addition of quantum dots into wide-bandgap perovskites' matrix, in addition to the valence and conduction bands of the perovskite. The introduction of such band allows greater absorption of photons, rising the theoretical maximum conversion efficiency up to 63.1 %.[13]

In wide-bandgap perovskites, the change in the bandgap energy from the replacement of iodine for bromide results in a change of colour, enabling wide-bandgap solar cells to, not only be used in energy harvesting applications, but also in building applications.[14] Since perovskite deposition and synthesis take place at low temperatures, it is suitable to be deposited on flexible substrates. Given that they are flexible, they can be easily integrated on small, large, and curved surfaces, and due to their lightweight they can be portable. All these features allow a wide range of applications. making PSCs an extremely attractive technology.[15]–[19]

1.3 Stability Drawbacks of Perovskite Materials

Despite all the advantages, there are drawbacks that limit its production scalability and commercialisation. Stability is the main issue because of how sensitive PCSs are to oxygen, moisture, temperature, and ultraviolet (UV) light, therefore accelerating its degradation rate, shortening its lifetime, and restricting its applicability.[3], [4] For these reasons, blocking all the harmful agents is extremely important.

1.3.1 Ultraviolet-Induced Degradation

UV photocatalytic degradation harms PSCs' performance on the long term significantly, and this is mainly caused by the ETL layer. The ETL layer has a higher energy bandgap than the absorber layer, hence, the UV radiation will be absorbed by it and generate an electron-hole pair, which will lead to the decomposition of the perovskite layer. As reported [20], TiO_2 has great capacity to extract electrons, and in the case of perovskite, it will target the halogen, leading to the formation of X^- at the ETL/perovskite interface, and afterwards the formation of X_2 resulting, consequently, in the degradation of the perovskite layer over time.

It also happens with SnO_2, even though in slower rate. The degradation mechanism is slightly different when compared with TiO_2. In a first stage, perovskite degrades into AX and BX_2., and this latter, after electron/hole pair generation separates, due to redox reactions, into B and X_2, which vastly harm the cells.[20]

1.3.2 Humidity-Induced Degradation

As for humidity, taking $MAPbI_3$ as example, it is stated that after 55 % relative humidity (RH) the degradation mechanism starts to take place, leading, eventually, primarily to the formation of PbI_2 precipitate, CH_3NH_2I and HI which are volatile, and the latter when exposed to oxygen and light results in H_2 and I_2.[21], [22] Nakamura et al. suggested that the mechanism involved is not that simple, being even different when cells are simultaneously exposed to light and humidity, forming CH_3NH_3I and $NH_4PbI_2{\bullet}H_2O$, and decomposing solely to PbI_2 when exposed only to humid environments.[23] Toloueinia et al. showed that the degradation rate is also dependent on the level of humidity, stating that at RH values lower than 80 %, the degradation is less pronounced but at higher values it becomes much more evident, confirmed by XRD analysis.[24]

1.3.3 Heat-Induced Degradation

From all the degradation sources, thermal degradation is harder to solve given the fact that when solar cells are exposed to sun light they will accumulate heat, which is difficult to avoid in solar harvesting applications, and consequently increase the degradation rate.[25]–[27] The A cation in a perovskite has great influence in the thermal stability of the films.[28] Moreover, not only does the perovskite layer influence the overall stability of PSCs, but also the HTL.[29]

1.4 Solutions to Stability Drawbacks

1.4.1 UV filters

To prevent-UV induced degradation, various strategies can be employed. These approaches include the use of UV filters [30][31], photoluminescence materials that downshift the absorbed light [32], or even interlayer materials [31] [33].

1.4.2 Encapsulation

Compared with other optoelectronic devices, PSCs fall behind in moisture and oxygen resistance research, as, for instance for LEDs (light-emitting diodes), encapsulants already protect devices from moisture and oxygen whilst having improved resistance to UV degradation and high transmittance.[34]

Water contact angle measurements show that films encapsulated are more hydrophobic than films without it, proving the moisture blocking ability of polymers, leading to longer lifetime of PSCs.[35] Additionally, UV-Vis absorption spectra display the clear steadier rate of degradation of encapsulated films, also supported by XRD and time-framed images of the films where a colour change from brown to yellow is noticeable in unencapsulated films, attributed to the formation of PbI_2.

Therefore, encapsulation is an obvious solution, but critical, as it enhances the stability of PSCs. One way to seal them is with thin film encapsulation (TFE), as the top sheet facing the sun, which can be deposited at low temperatures and prevent moisture from entering the cell. Humidity and oxygen can also infiltrate from the sides of the solar cell, and for long-term stability it must be kept to a minimum. Epoxy resins are used as edge seals, and in combination with TFE, PSCs show great resistance to oxygen and moisture.[36]

However, for thin film solar cells, flexible applications are extremely attractive, but rigid encapsulation cannot be applied for flexible solar cells, and since flexible encapsulation is not as good as rigid, other alternatives must be found so that PSCs technology can fully reach its potential.

1.4.3 Widening the Perovskite Bandgap with Br incorporation

As aforementioned, by substituting the halide element in perovskite, one can change its properties, such as bandgap energy. Besides those, the substitution enhances PSCs' stability, increasing their lifetime. When substituting iodine for bromine in $MAPbX_3$ (X=I, Br), besides the increase on E_G, there is also a natural increase in stability given the fact the halide ion migration is supressed, consequently inhibiting MA^+ migration.[37] Even when mixing these halides in $MAPb(I_{1-x}Br_x)_3$ perovskites, XRD data shows that with iodide the degradation rate is much higher than that of perovskites with bromide, where over time, when exposed to light and air, peaks related to PbI_2 become more relevant.[9], [38] Therefore, the stability of PSCs can be enhanced by using wider-bandgap perovskites materials.

1.4.4 Quantum Dots Inclusion

Another solution to solve the stability problem of perovskite materials is by incorporating colloidal quantum dots (QDs), in small concentrations, in our solar cells. Lead sulphide (PbS) QDs, just like perovskites, show great properties, such as high absorption coefficient, and high air stability, which make them an interesting subject to study.[39] They can not only be used to fabricate solar cells where they act as the absorber layer, but also as a passivation layer when in the perovskite matrix or as a layer between the perovskite and ETL and HTL, which enhances the PSCs' stability.[40]–[42] When incorporated in the interfaces as a passivation layer, it helps reducing the photocatalytic effect of the metallic oxide material's degradation, and prevents moisture induced degradation.[43], [44]

In-matrix PbS-QDs serve as seeding sites that promote perovskite crystal formation as seen in Figure 2, resulting in significant improvements in morphology in terms of grain size, surface coverage, and uniformity.[39], [45] Moreover, because of the strong interactions with the perovskite's halide material, ion migration is highly inhibited, which prevents perovskite degradation, as its incorporation leads to a reduction in Pb^{2+} dangling bonds, since the sulphide present on PbS bonds to Pb atoms in perovskite crystal. Ultimately, all these factors result in better overall performances of PSCs, but most importantly an increase in stability.

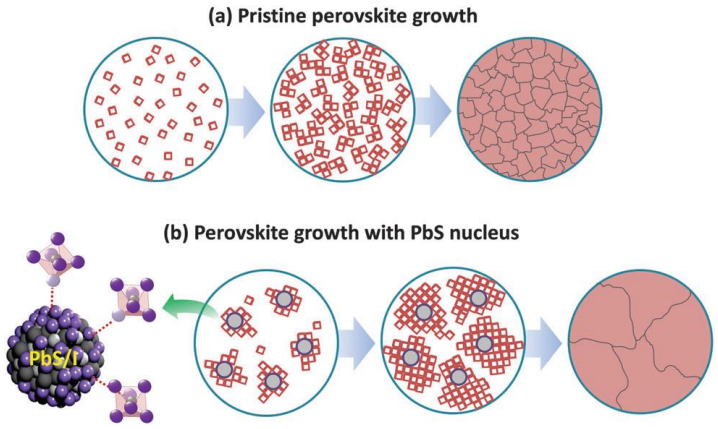

Figure 2. Proposed nucleation and growth routes of perovskite crystal thin films without(a) and with (b) MAI-capped PbS nanoparticles.[45]

Additionally, QDs are also extremely attractive to fabricate intermediate band solar cells (IBSCs).[12], [46], [47]

1.5 Air Processed Perovskites

Apart from efficiency and stability, which have been the main the focus when studying PSCs in the last decade, something that is also fundamental to consider is its manufacturing process, in particular when considering its

commercialisation. Being able to fabricate PSCs, or any solar cell, without the need to rely on complex and expensive systems, and that do not involve high temperatures or vacuum systems, is of extreme importance. Because of this, air-processing is crucial. However, is more complex and challenging than conventional glove-box (GB) processing, since ambient conditions, especially RH and ambient temperature, are not well-controlled.[48] This humidity variation during the deposition of perovskite leads to a nonuniform surface and the formation of pinholes. Moreover, the volume and especially the timing of the antisolvent dropping, highly affects the film's quality, making it more difficult to reproduce.[49] To overcome this issue, Chao et al. managed to fabricate devices in ambient air with high RH (>80 %) via one-step deposition method without the need of an antisolvent.[50] By substituting the commonly used solvents, dimethylformamide (DMF) and dimethyl sulfoxide (DMSO), for methylammonium acetate (MAAc), it was possible to fabricate antisolvent-free perovskites with good quality, and corresponding devices achieving a maximum PCE 20.05 %. Furthermore, the deposition of wide-bandgap PSCs in ambient air has also been reported, with cells keeping 80 % of their initial PCE value after 3500 h.[51]

Additionally, in order to commercialise PSCs, it is necessary to produce such devices in large areas, and this is not possible by spin-coating. Slot-die coating is one the most studied techniques for this matter and considered really promising given the fact that can be integrated into a roll-to-roll system.[52]

1.5.1 One-Step Deposition Method

When it comes to depositing perovskite films, it can be done following a one-step, or a two-step deposition method. Following the one-step deposition method, both organic and inorganic precursors are mixed in one solution that it is deposited to synthetise the perovskite film. This process requires dispensing of an antisolvent, which is crucial to the perovskite crystallisation process. It helps forming a uniform pin-hole free perovskite film. However, the volume and the time when the antisolvent is dispensed are two major parameters that must be controlled according to the lab's temperature and humidity. To eliminate this dependency, an antisolvent-free one-step deposition has been studied, producing high-quality films without the need for an antisolvent washing process.[53] Overall, the one-step deposition approach is the most used given its simplicity and the fact that is less time consuming, but, as just mentioned, its high dependence on the antisolvent reducing its reproducibility is a drawback of this method.

1.5.2 Two-step Deposition Method

On the other hand, the two-step deposition method does not require the antisolvent washing step. For this method, two solutions are used, one containing the inorganic precursor and the other containing the inorganic precursor, $PbBr_2$ and MABr respectively, taking $MAPbBr_3$ as an example. To synthetise perovskite films by two-step deposition method, first the inorganic precursor is deposited, followed by the organic precursor. The fact that antisolvent is not used greatly helps the process' reproducibility, even though it is more time consuming when compared to the one-step method. Nonetheless, this approach also presents its disadvantages. Due to the fact that $PbBr_2$ is firstly deposited, MABr that is deposited afterwards has some difficulty diffusing through it, resulting in an incomplete reaction of the precursors.[54] Therefore, $PbBr_2$ residues are visible by SEM and XRD analysis, which, consequently, negatively affect the perovskite film and PSCs performance. All in all, the two-step approach is much less studied, which makes this method not as optimised as the one-step method.

2

MATERIALS AND METHODS

2.1 Device Preparation

To fabricate devices, ITO coated glasses (15 Ω/sq, Xin Yan Technology LTD) are used as the substrate with dimensions of 2.5×2.5 cm^2. Afterwards, they are cleaned according to the procedure in appendix section A1. After the procedure, they are dried with compressed air (N_2), and taped with Kapton tape before being submitted to an ultraviolet/ozone treatment (UV/O) for 15 min.

2.2 ETL Deposition processes

2.2.1 SnO_2 Deposition

To deposit the SnO_2, 5 droplets of an undiluted SnO_2 solution (Tin(IV) oxide 15% in water, colloidal dispersion, Fisher Scientific) filtered by a 0.22 μm filter are spin-coated at 3000 rpm (2000 rpm/s acceleration) for 30 s (Laurell WS-400-6NPP-LITE). The films are then placed on a hotplate at 120 ℃ for 10 min and annealed for 30 min on a desiccator at 170 ℃ under vacuum.

2.2.2 TiO_2 Deposition

2.2.2.1 Compact Layer (c-TiO_2)

For the c-TiO_2 layer, two solutions are prepared (described in appendix section A2) and mixed. From the resulting solution, 125 μL are spin-coated at 4000 rpm (2000 rpm/s acceleration) for 30 s. Then, the films are placed on a hotplate for 10 min at 120 ℃ and annealed for 30 min at 550 ℃ in a furnace.

2.2.2.2 Mesoporous Layer (m- TiO_2)

For the m-TiO_2 layer, 135 μL of m-TiO_2 solution (preparation described in appendix section A3) are spin-coated at 4000 rpm (2000 rpm/s acceleration) for 12 s. The films are placed on a hotplate for 5 min at 100 ℃ and annealed for 30 min at 450 ℃ in a furnace. The films are afterwards submitted to an UV/O treatment before the perovskite deposition, 30 min for SnO_2 films, and 15 min for TiO_2.

2.3 Perovskite Layer Fabrication

2.3.1 One-Step Deposition Method of $MAPbBr_3$

From $MAPbBr_3$ precursor solution (preparation described in appendix section A4), 110 μL are spin-coated at 2000 rpm (2000 rpm/s acceleration) for 10 s as the first spin rate, and at 5000 rpm (3000 rpm/s acceleration) for 20 s as the second spin rate, followed by the dispensing of 120 μL of chlorobenzene (99.8%, Extra Dry, AcroSeal™, Thermo Scientific Chemicals, Fisher Scientific) as soon as the rotation reaches 5000 rpm (last 17.5 s). The films are annealed at 120 ℃ for 15 min.

2.3.2 Two-Step Deposition Method of $MAPbBr_3$

Firstly, 110 μL of $PbBr_2$ solution are spin-coated at 2000 rpm (2000 rpm/s acceleration) for 10 s as the first spin rate, and at 5000 rpm (3000 rpm/s acceleration) for 30 s as the second spin rate. The films are annealed at 70 ℃ for 5 min and let to cool down to room temperature. Afterwards, 110 μL of MABr solution are spin-coated at 4000 rpm (2000 rpm/s acceleration) for 20 s. The films are annealed at 100 ℃ for 10 min. Solution fabrication in appendix section A5.

2.4 QD Addition to Perovskite Precursor Solution

After a ligand exchange procedure (appendix section A6) the QDs are dried in vacuum for 30 min and are dispersed in the perovskite solution.

2.5 HTL Deposition

Right after the perovskite layer cools downs to room temperature, Spiro-MeOTAD (preparation described in appendix section A7) is spin-coated at 2000 rpm for 30 s.

2.6 Back Contact deposition

To complete the cell, gold is deposited by electron beam (e-beam) vapor deposition over a mask with 2×5 mm^2 opening. All depositions, besides the gold evaporation, were done outside of the GB.

2.7 Characterisation Methods

The techniques used to characterise the fabricated films and devices are described in appendix section B.

3

RESULTS AND DISCUSSION

Wide-bandgap perovskite materials can be applied in many fields, and not only for solar harvesting applications. For instance there is now great interest in tandem solar cells (e.g. perovskite-on-silicon), CO_2 reduction devices, or intermediate band solar cells (IBSC) [10]–[12], as well as to building applications [14], as mentioned in the Introduction section 1.2. Given also their potential to enhance the stability of PSCs, as referred in the Introduction section 1.4.3, here we studied a wide-bandgap (2.30 eV) material, $MAPbBr_3$.[37] In the first part of this work $MAPbBr_3$ films and devices were developed in ambient air. To further improve PSCs stability, when then explored the incorporation of QDs into the perovskite matrix, as sketched in Figure 2, when inserted at the right concentration the QDs can act as distributed nucleation sites assisting the crystallisation of the perovskite film. Besides, due to their strong interaction with the perovskite lattice, ion migration is further reduced, and there is also a decrease in the dangling bonds density in the perovskite, as stated in Introduction section 1.4.4.[39] Therefore, after the development of good films and solar cells in ambient air, the stability of $MAPbBr_3$ devices with and without QDs was assessed.

3.1 Development of Wide-Bandgap Perovskite Solar Cells

The deposition procedure of low-bandgap perovskites is already optimised given the extensive research in the last decade, with fabricated cells matching the record efficiency of silicon base devices, as stated in the Introduction section 1.1. On the other hand, far less researched, wide-bandgap perovskites' deposition procedure is far from optimised, especially in ambient air [51]. Thus, in this work, we started by studying the ambient air-deposition of the perovskite layer via two different approaches, one-step and two-step, whilst varying some parameters, such as the concentration of precursor solutions and the solution solvent ratio, in order to fabricate devices with the best quality possible. Later an additive was tested since, according to literature [55], it improves the perovskite structural and optical properties.

3.1.1 One-Step Deposition Method

3.1.1.1 Concentration Study

Before studying the perovskite stability and the influence of the introduction of QDs in the perovskite matrix, it was essential to develop good quality $MAPbBr_3$ films. For the one-step deposition method, three different concentrations were tested: 0.6 M, 0.8 M, and 1.0 M. As for the antisolvent, chlorobenzene was chosen.

In order to study the films' morphology, the three concentrations were deposited on ITO coated glass. Analysing the SEM images of $MAPbBr_3$ films for the first time was challenging, due to the fact that the films would crack instantly by the electron beam at the grain boundaries and overtime these would grow to a size

where it would be impossible to analyse them. To solve this issue, it is suggested that decreasing the voltage and the current of the incident electron beam helps reducing this effect.[56] After decreasing the incident beam's voltage cracking would still occur, but at a slower rate, making the analysis possible. Looking at the SEM images in Figure 3, the cracking effect is visible, especially on the 0.8 M film. Even though all three films show good surface coverage, pinholes are visible on 0.6 M and 0.8 M films. The 1.0 M film clearly distinguishes itself from the other two concentrations, as it is much more compact and uniform. Also, as the precursor solution concentration increases, the grain size and its distribution also increase, averaging 359.87 ± 93.04 nm, 408.56 ± 99.25 nm, and 627.13 ± 224.97 nm for 0.6 M, 0.8 M, and 1.0 M, respectively.

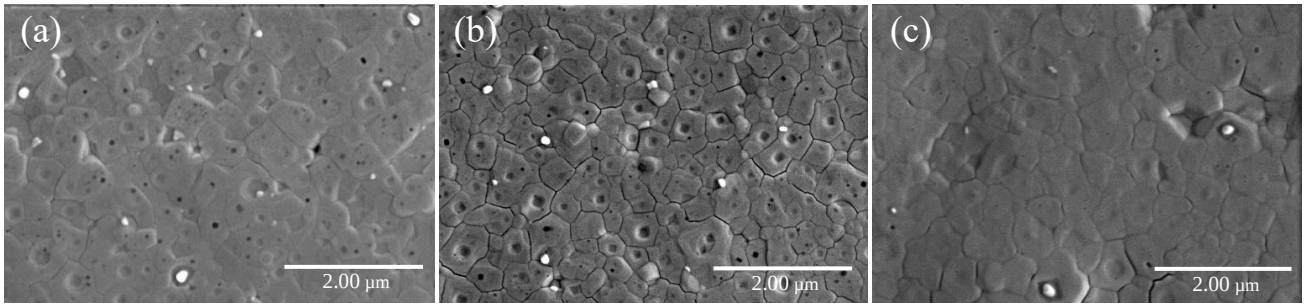

Figure 3. SEM images and grain size distribution of one-step $MAPbBr_3$ films prepared with 0.6 M (a), 0.8 M (b), and 1.0 M (c) precursor solutions, respectively.

For the XRD analysis, films were deposited on glass, and the obtained XRD data confirms the formation of $MAPbBr_3$, as the main diffraction peaks can be seen at 14.90°, 30.09°, and at 45.86° in Figure 4 which correspond to (100), (200), and (300) planes of the $MAPbBr_3$'s cubic structure, respectively, and indicate the growth preference in the ⟨100⟩ direction.[57] It can be seen that the crystallinity degree follows a increasing trend with the increase in concentration, as the diffraction intensity is higher for higher precursor solution

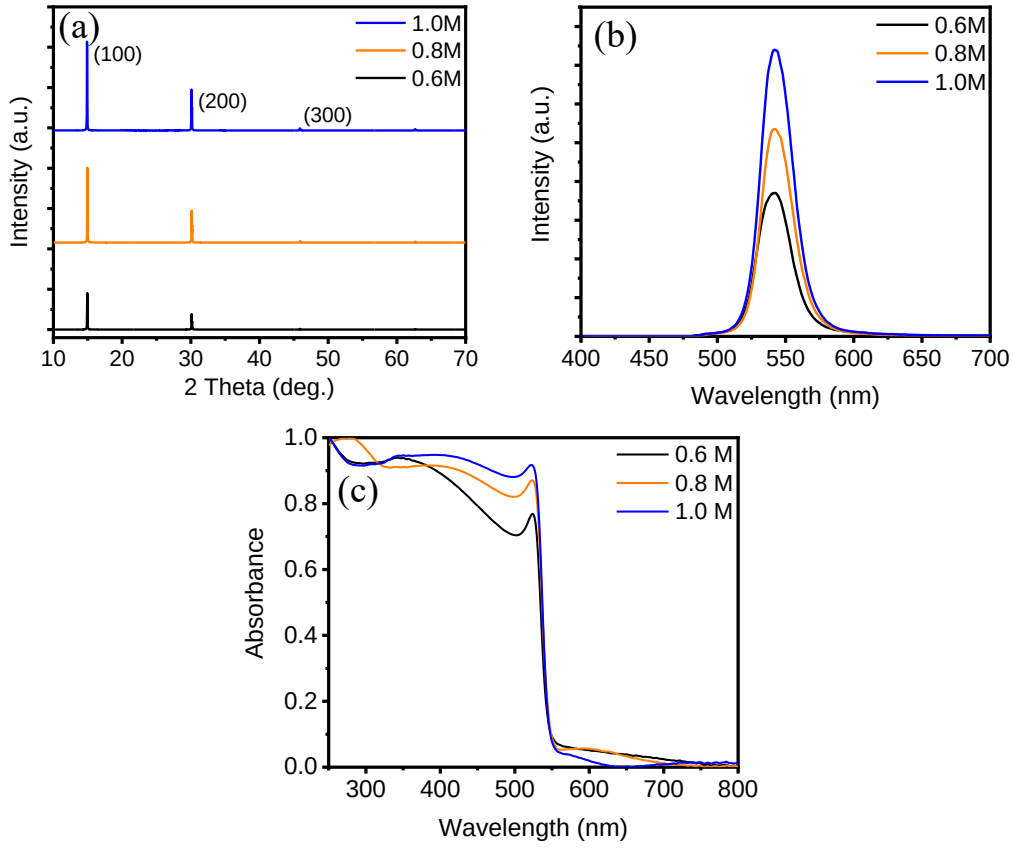

Figure 4. XRD (a) PL spectra (b) and absorbance spectra (c) of one-step $MAPbBr_3$ films prepared 0.6 M, 0.8 M, and 1.0 M precursor solutions.

concentrations. Therefore the 1.0 M precursor solution produced the most crystalline films, and 0.6 M the least crystalline.

Not only 1.0 M films show more intense peaks in the XRD analysis, but they also do in PL, as seen in Figure 4. As the precursor solution concentration increases, the emission peak intensity increases and, possibly, the full width at half maximum (FWHM) gets smaller, which indicates the formation of films with lower trap density. Since 0.6 M film has the lowest peak intensity, it has more defects leading to recombination of the generated charges though defect levels. On the other hand, as 1.0 M film peak is more intense, the recombination is more radiative. But 1.0 M precursor solutions do not necessarily yield perovskite films of higher quality, as the films thickness increases with the concentration of the precursor solution (0.6 M, 0.8 M, and 1.0 M films are 313.00 ± 18.81 nm, 365.67 ± 25.03 nm, and 416.00 ± 2.65 nm thick, respectively). Thicker films are expected to exhibit more intense emission peaks.

When analysing the UV-Vis spectrum presented in Figure 4, thickness has also to be considered since it influences the absorbance of the films. Since for the synthesis conditions 1.0 M films are thicker, which leads to greater absorbance, they are more suitable to fabricate devices. However, similarly to the PL analysis, it cannot be directly said that 1.0 M films are optically better than 0.8 M and 0.6 M films when it comes to absorption. $MAPbBr_3$ films start to absorb incident light at 539.5 nm, which corresponds to a bandgap energy of 2.30 eV, according to Tauc plots presented in the appendix section C Figure 22, matching the bandgap energy value in literature.[57] The absorbance spectra of the films, presented in Figure 4, confirms that $MAPbBr_3$ has a direct bandgap, since it rises sharply with wavelength decrease, meaning that in order to absorb a photon no assist from lattice vibration is required, contrary to silicon, that since it has an indirect bandgap, a phonon is necessary for the charge carrier generation.

3.1.1.2 Perovskite Precursor Solution Solvent Ratio Study

In addition to concentration, solvent ratio (DMF/DMSO v:v) was studied as well. As mentioned in the Introduction section 1.5, DMF and DMSO are the most used solvents, and are mixed together in various ratios, being 7:3 and 9:1 frequently used.[3]–[5] Therefore, in order to find the best solvent ratio to be used in our experiments, three different ratios were investigated: DMF/DMSO 1:0, DMF/DMSO 9:1, and DMF/DMSO 7:3. In this study, the films were deposited at 25.5 °C, which is considerably a high temperature for optimal perovskite deposition, making the synthesis more challenging.

From the UV-Vis analysis, in Figure 5 it is clear to see that DMF/DMSO 7:3 film shows higher absorbance than the other two ratios, which have similar absorbance peak intensity. This is explained by their thicknesses because, as DMSO volume increases the thickness also rises. Films synthesised with solely DMF are on average 353.00 ± 7.87 nm thick, and films synthesised with DMF/DMSO 9:1 are on average

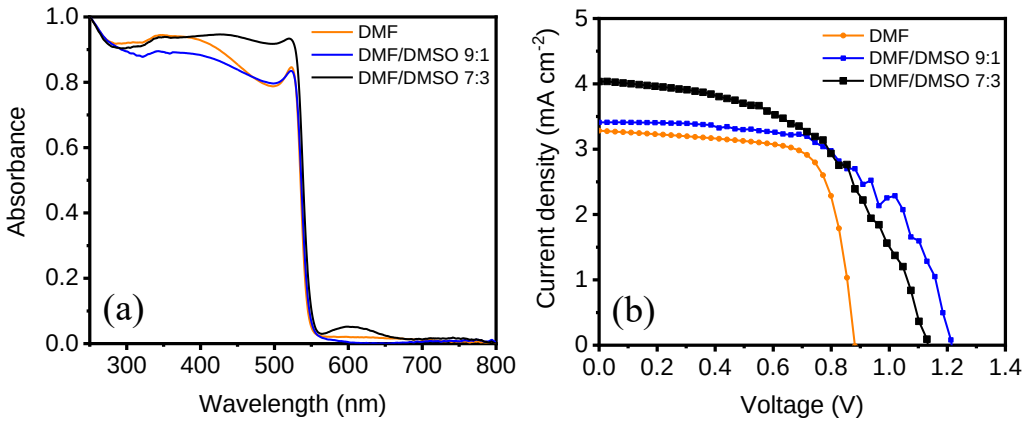

Figure 5. Absorbance spectra (a) and J-V curves (b) of $MAPbBr_3$ films and devices synthesised via one-step using DMF/DMSO 1:0, DMF/DMSO 9:1 and DMF/DMSO 7:3 ratios for the precursor solutions.

358.00 ± 14.02 nm thick. Given that their thicknesses are similar, they have comparable absorbance. Only for wavelengths shorter than 400 nm DMF/DMSO 1:0 films present higher absorbance. However, in a solar cell, higher energetic wavelengths are absorbed by the ETL, therefore, the greater absorbance of DMF/DMSO 1:0 in such part of the spectrum is not relevant. Regarding DMF/DMSO 7:3 films, they are on average 418.50 ± 34.64 nm thick, much thicker than the other films, which leads to higher absorbance. Additionally, no change on the bandgap is visible with addition of DMSO to DMF as seen in appendix section C Figure 23.

Moreover, to assess the PV performance, solar cells were fabricated with the three different ratios, with structure as follows: ITO/c-TiO_2/m-TiO_2/$MAPbBr_3$ (1.0 M)/Spiro-MeOTAD/Au. The J-V plots of the cells with higher PCE of mentioned PSCs are presented in Figure 5, and the PV parameters are displayed in Table 1. Cells fabricated with solely DMF have the lowest PCE of 2.09 % (V_{OC} = 0.88 V, J_{SC} = 3.28 mA/cm^2, FF = 72.23 %), followed by DMF/DMSO 9:1 with 2.12 % (V_{OC} = 1.12 V, J_{SC} = 3.24 mA/cm^2, FF = 58.66 %) and finally DMF/DMSO 7:3 with 2.42 % (V_{OC} = 1.13 V, J_{SC} = 4.05 mA/cm^2, FF = 53.17 %). In the box charts presented in Figure 6, cells fabricated with only DMF average really low values for V_{OC}. It is relevant to point it out when working with wide-bandgap solar cells, as they are characterised by outputting high V_{OC}'s, being 1.653 V, the record V_{OC} obtained with $MAPbBr_3$ as the absorber material.[4] It did not happen when solvents were mixed as cells achieve V_{OC} values as high as 1.21 V and 1.26 V for DMF/DMSO 9:1 and DMF/DMSO 7:3, respectively, despite these two values still being far from the theoretical maximum of 1.963 V (for E_G = 2.30 eV).[6] However, using only DMF as solvent does not justify such low V_{OC} values. As mentioned before, the temperature was over 25 °C, and it was noticed that as ambient air temperature increased the depositions became more inconsistent. This led to the formation of bad hazy $MAPbBr_3$ films, which is totally undesirable. This can be seen in the box charts in Figure 6 as DMF and DMF/DMSO 7:3 devices' parameters have high deviations. For these reasons, DMF/DMSO 9:1 was chosen as the solvent mix to be used, since, from all the solvents ratios, the devices fabricated with such ratio have the lowest deviation, allowing for better reproducibility in ambient air, despite DMF/DMSO 7:3 films having higher absorbance and producing the most efficient device.

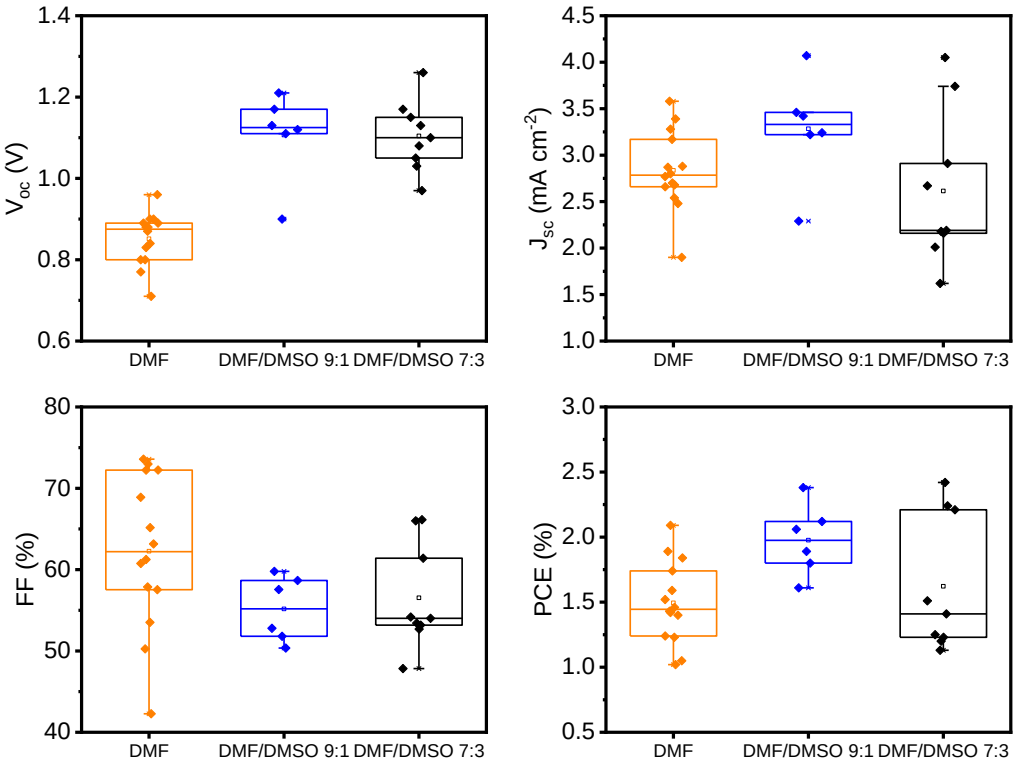

Figure 6. Box charts of the photovoltaic parameters obtained at reverse scan of $MAPbBr_3$ devices fabricated via one-step with different solvent ratios.

Table 1. Photovoltaic parameters of solar cells fabricated via one-step with different solvent ratios.

Solvent	V_{OC} (V)	J_{SC} (mA/cm^2)	FF (%)	PCE (%)
DMF	0.88	3.28	72.23	2.09
DMF/DMSO 9:1	1.12	3.24	58.66	2.12
DMF/DMSO 7:3	1.13	4.05	53.17	2.42

To summarise, for the one-step deposition approach, given the better results obtained, $MAPbBr_3$ precursor solutions are prepared with a 1.0 M concentration in DMF/DMSO 9:1.

3.1.2 Two-Step Deposition Method

3.1.2.1 Precursors Solutions' Concentration Study

Regarding the two-step deposition method, the same precursor solution concentrations were tested. Since the films are deposited via two-step method, there is no need to use an antisolvent.

Concerning the films' morphology, the three concentrations were deposited on ITO coated glass. Contrary to the one-step method, the two-step deposition approach synthesised $MAPbBr_3$ nanocubes as seen in Figure 7. Additionally, two-step films show poor surface coverage and, interestingly, it gets worse as the concentration gets higher, opposite to the one-step method. One possible reason to why this happens, is that higher precursor solution concentrations form an initial more compact layer of $PbBr_2$, and when MABr is dispensed, it is harder for it to diffuse into the initial $PbBr_2$ layer. For smaller concentrations, on the other hand, MABr can penetrate more easily and synthesise higher quality perovskite films.[54] Therefore, 0.6 M had better overall morphology, followed by 0.8 M and by 1.0 M. Grain size measurements also reinforce this idea, since the 0.6 M solution synthesised bigger cubes (270.73 ± 127.12 nm) with bigger size distribution than the other two concentrations (170.91 ± 83.96 nm for 0.8 M, and 163.86 ± 52.24 nm for 1.0 M). Moreover, big sized residues, which correspond to unreacted $PbBr_2$ confirmed by EDX analysis (appendix section C Figure 24), are visible and get more notorious as the precursor solution concentration increases.

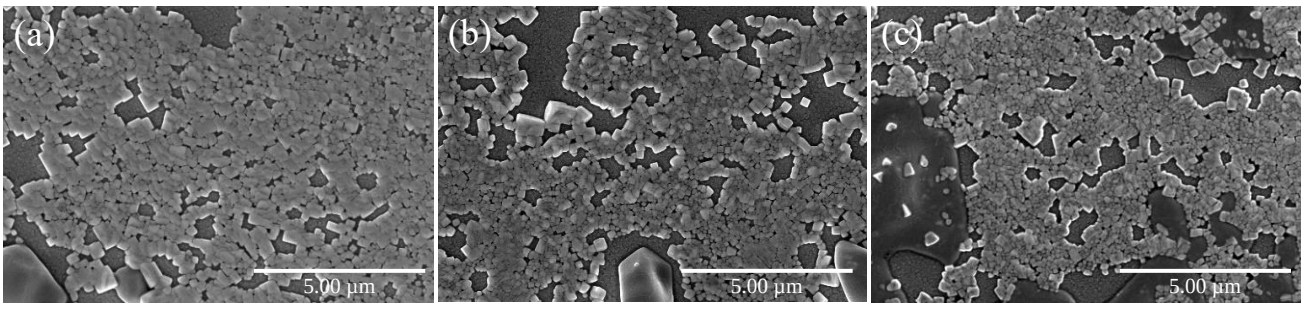

Figure 7. SEM images and grain size distribution of two-step $MAPbBr_3$ films prepared 0.6 M (a), 0.8 M (b), and 1.0 M (c) precursor solutions, respectively.

XRD analysis was not conducted, and it would help to identify $PbBr_2$ diffraction peaks. If conducted, the main diffraction peak would be visible at around 12.2°.[58], [59]

From PL analysis seen in Figure 8, 0.6 M film achieved the best optical results, as it shows a more intense emission peak when compared to 0.8 M, and 1.0 M, which show similar intensities. This confirms the better quality of films fabricated with lower concentrated precursor solutions via two-step deposition method, as seen in the SEM images. Therefore, as the precursor concentration increases, the trap density also increases, resulting in less radiative recombination since the charges start to recombine through defect levels. However, the greater intensity can also be explained by the thickness of the films just like in the one-step deposition method study, as 0.6 M, 0.8 M, and 1.0 M films are 358.50 ± 29.66 nm, 310.00 ± 17.68 nm, and 309.50 ± 15.10 nm thick, respectively. The similar emission peak intensity between 0.8 M and 1.0 M films is

possibly due to saturated $PbBr_2$ solutions, since, after stirring overnight, there was still undissolved powder sitting on the bottom of the vials, meaning that 0.8 M and 1.0 M solutions had more or less the same concentration leading to close films' properties. This closeness can also be noticed when comparing the average grain size of the films in Figure 7. Although 1.0 M produced overall smaller grains, their size is close to 0.8 M's grains. Comparing with 0.6 M, a big gap between sizes is very noticeable. This issue happens because $PbBr_2$ does not dissolve well in DMF, and can be solved by adding small concentrations of MABr to the inorganic precursor solution. [60]

The absorbance spectra presented in Figure 8 show again that 0.6 M precursor solution, produced higher quality films, having better optical properties. Although in the PL graph, 0.8 M and 1.0 M had similar results, when it comes to the absorbance analysis, 0.8 M performed slightly better, which in a way can be explained by the SEM images, since as the concentration of the precursor solution increases, the film quality decreases. Not only this, but the films are not fully homogeneous and, thus, the placement of the films in a slightly different position on the equipment leads to the analysis of areas of the films with slightly different quality. All the films have a bandgap energy of 2.30 eV as seen in appendix section C Figure 25, and even though the quality of the films is not the best, the formation of $MAPbBr_3$ was successful on all of them.

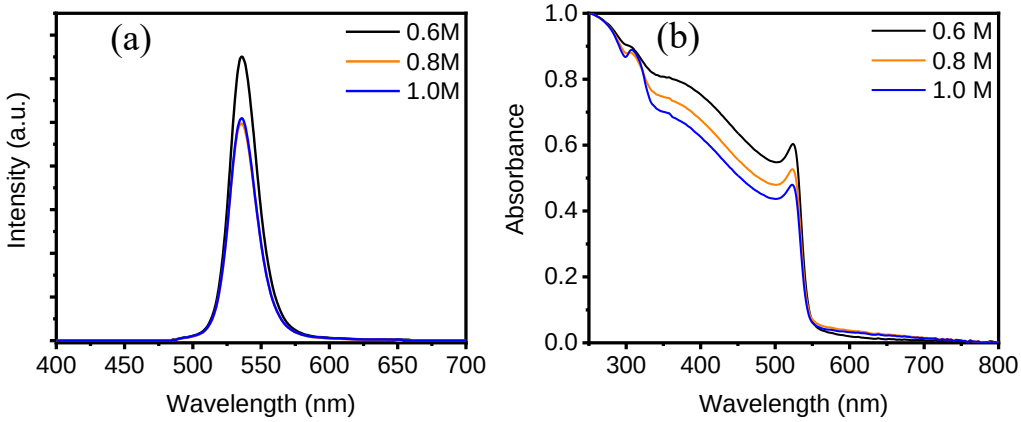

Figure 8. PL spectra (a) and absorbance spectra (b) of two-step $MAPbBr_3$ films prepared with 0.6 M, 0.8 M, and 1.0 M precursor solutions.

3.1.2.2 Ratio Study of Organic and Inorganic Components

Given that the concentrations investigated did not yield quality films due to low surface coverage and the fact that precursor residues were present on the films, a ratio analysis was conducted.

When it comes to the two-step deposition method, 1:1 ratio between precursors ($PbBr_2$:MABr) is not used in many research reports. It is common to use a ratio close to 1:0.27 instead of 1:1, although other ratios are also used. For instance, for 1 M of $PbBr_2$, concentrations of MABr ranging from 5 mg/mL up to 75 mg/mL (0.04 M up to 0.67 M) have been investigated.[61] For this reason, in this thesis, 1:0.27 ratio was studied in addition to 1:1 ratio. The concentration of $PbBr_2$ was defined as 1.0 M and MABr as 0.27 M (30 mg/mL).

The SEM image in Figure 9 show the formation of nanocubes, which were also synthesised via two-step using 1:0.27 ratio. For the lower concentration of the organic component, a big improvement on surface coverage is achieved when compared with 1:1 ratio. Additionally, there are no visible $PbBr_2$ residues, meaning that the reduction of MABr concentration compared to that of $PbBr_2$ helps the formation of $MAPbBr_3$ films. Thus, although, some pinholes are visible, an improvement in morphology was achieved by changing the ratio between precursors. This may happen because with high concentration of MABr, more $MAPbBr_3$ is crystallised in an initial phase obstructing the diffusion of MABr leading to uncomplete reaction of $PbBr_2$. But when MABr concentration decreases in relation to that of $PbBr_2$, less $MAPbBr_3$ crystallises at the top of the initial $PbBr_2$ layer and MABr can diffuse more easily.

The XRD analysis in Figure 9 shows that the formation of $MAPbBr_3$ was successful. However, when comparing with the one-step XRD results, many more diffractions peaks are visible. In addition to (100), (200), and (300) planes, (110), (210), (211) and (220) located at 21.09°, 33.70°, 37.04°, and 43.05°, respectively, are also spotted. [62] Although the film still grows preferably in the ⟨100⟩, the appearance of more phases suggests that it is more polycrystalline than the films synthesised via one-step. Nevertheless, no peaks related to $PbBr_2$ were detected, which is a good indicator that a better-quality film was synthesised. However, compared to the one-step films, the intensity of the diffraction peaks is much lower, given its polycrystallinity as seen in appendix section C Figure 26.

Additionally, the optical properties of films synthesised with different ratios were compared. Looking at the UV-Vis spectra in Figure 9, the difference between films is clear. Films synthesised with a 1:0.27 ratio are of higher quality and more suitable for solar harvesting applications has they absorb more of the incoming light.

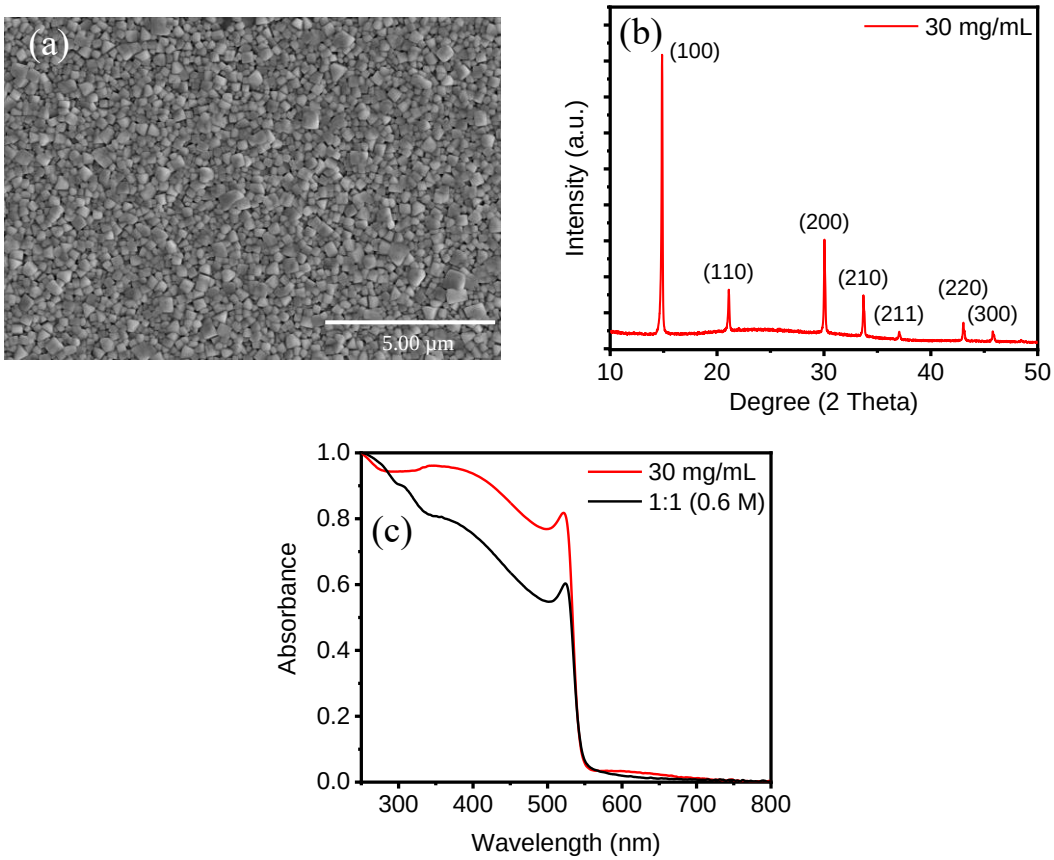

Figure 9. SEM (a) and XRD (b) of two-step 1:0.27 $MAPbBr_3$ films; absorbance spectra of two-step $MAPbBr_3$ films fabricated with 1:0.27 (red) and with 1:1 (black) ratios precursor solutions (c).

3.1.3 One-Step vs Two-Step PV Performance

In order to assess and compare devices' PV performance, solar cells were fabricated via one-step and two-step deposition methods. To deposit the perovskite layer, for the one-step method a 1.0 M precursor solution (DMF/DMSO 9:1) was used, and for the two-step approach, 1:0.27 ratio was used (1.0 M and 0.27 M for $PbBr_2$ and MABr, respectively). The devices' structure was as follows: ITO/SnO_2/$MAPbBr_3$/Spiro-MeOTAD/Au as seen in Figure 10. The J-V plots of fabricated solar cells are presented in Figure 11, and the PV parameters in Table 2. The box charts of the PV parameters displayed in appendix section D Figure 30, show that, on average, one-step devices achieved higher PCE than two-step devices, even though two-step films have higher V_{OC} value. The maximum achieved PCE by one-step devices was 2.23 % (V_{OC} = 1.21 V,

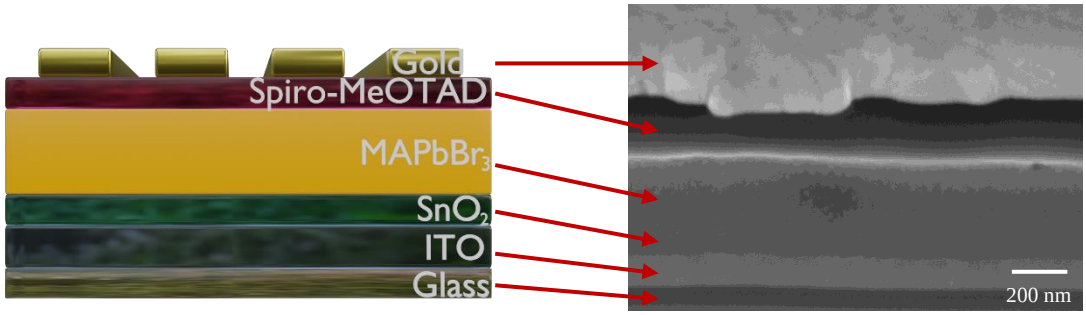

Figure 10. SEM images showing a cross-section of an ITO/SnO_2/$MAPbBr_3$/Spiro-MeOTAD/Au solar cell.

J_{SC} = 3.05 mA/cm^2, FF = 60.55 %), whereas the maximum achieved PCE by two-step devices was 1.57 % (V_{OC} = 1.21 V, J_{SC} = 3.05 mA/cm^2, FF = 60.55 %). This discrepancy can be explained by the major difference in J_{SC}, which is clarified by the films' absorbance spectrum seen in Figure 11. Two-step films when compared with on-step ones, show lower absorbance, which, therefore, translates to lower photocurrent.

Table 2. Photovoltaic parameters of solar cells fabricated via one-step (1.0 M) and two-step (1:0.27) measured after fabrication.

Deposition Method	V_{OC} (V)	J_{SC} (mA/cm^2)	FF (%)	PCE (%)
One-step	1.21	3.05	60.55	2.23
Two-step	1.33	1.88	62.52	1.57

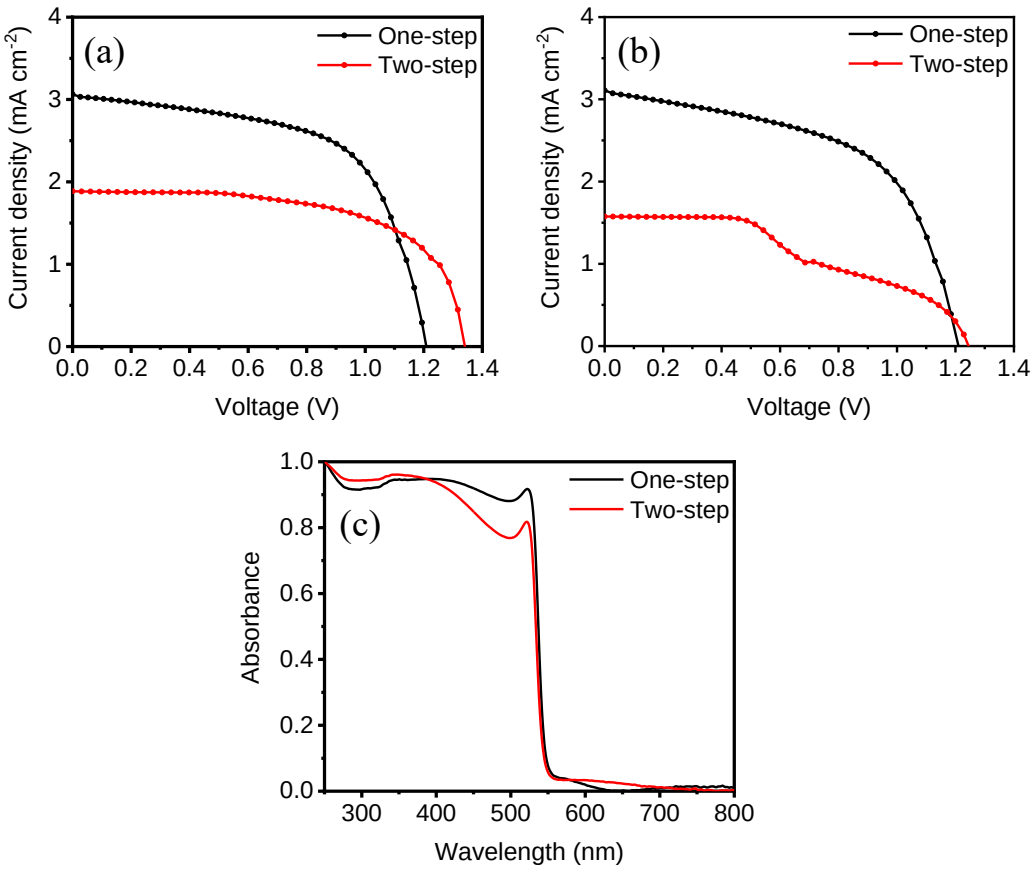

Figure 11. J-V curves of $MAPbBr_3$ devices synthesised via one-step (1.0 M) and two-step (1:0.27) measured after fabrication (a) and after 360 h; Absorbance spectra of $MAPbBr_3$ films deposited via one-step (1.0 M) and two-step (1:0.27) (c)

From the first measurements, one-step devices performed better than two-step ones. But, apart from the initial PV performance, the stability assessment of the devices was also performed. After 360 h, the PV performance of the best devices was measured once again. The new J-V plots and parameters are presented in Figure 11 and Table 3, respectively. It is seen that after 360 h, regardless of the deposition method both devices degrade, as their PCE drops. However, the degradation is much more significant for the two-step device, as its PCE dropped from 1.57 % to 0.76 %, corresponding to 51.6 % loss. Its J-V curve lost it initial shape, and led to a massive drop in FF, because of the rise on the series resistance. On the other hand, after 360 h, the one-step device maintained 93.27 % of its initial PCE value.

Therefore, based on these results, for the optimised conditions, one-step deposition method results in higher quality films when compared to the two-step approach, which allow the fabrication of more efficient and stable devices. For these reasons, one-step deposition approach is solely used for the rest of this work.

Table 3. Photovoltaic parameters of $MAPbBr_3$ solar cells fabricated via one-step (1.0 M) and two-step (1:0.27) measured 360 h after fabrication.

Absorber layer	V_{OC} (V)	J_{SC} (mA/cm2)	FF (%)	PCE (%)	PCE loss (%)
One-step	1.21	3.10	55.58	2.08	6.73
Two-step	1.24	1.57	38.80	0.76	51.6

3.1.4 Additive Test in Perovskite Precursor Solution

The synthesised $MAPbBr_3$ films with higher quality were prepared with 1.0 M precursor solution via one-step deposition method. Nevertheless, the PV parameters were still low, especially J_{SC}. For this reason, to enhance the perovskite absorber layer properties, and thus cell performance, one additive represented in literature [55] was investigated in this thesis. It is a type of an organic compound, 4-tert-butylpyridine (pyridine), mostly applied to the well-known HTL Spiro-MeOTAD. The addition of pyridine to the perovskite layer can lead to an increase in V_{OC} and potentially in J_{SC}, since pyridine helps to suppress the crystallographic defects originated from dangling bonds. It also enhances the overall film's quality, controlling the nucleation process by retarding the growth of the perovskite, which will lead to fewer lattice defects. Hence, improving the overall quality of the active layer and, consequently, improving the device's performance. In this section, pyridine is used as an additive in a concentration of 5 % of the solvent volume of the perovskite solution (corresponding to 0.34 M).

Regarding the films' morphology, Figure 12 displays the SEM images of the synthesised films. When pyridine is not added, the synthetised films have the same morphology as the films deposited on the One-Step Deposition section 3.1.1, showing a compact film with good surface coverage, although some pinholes and some small cracks are visible, due to the incident electron beam. But when pyridine is added, the film's surface has more pinholes, which are harmful for the solar cells in various ways. By reducing the effective area of the absorber layer less light is absorbed and, consequently reducing the photogenerated current. In addition, pinholes may create paths for the current to bypass the active area, leading to a decrease in shunt resistance, decreasing the current density. Nevertheless, despite the pinholes, pyridine appears to have a positive influence on the film's morphology, since the film's surface is more uniform when compared with pristine films.

Looking at the PL spectra in Figure 12 and comparing pristine films with films where pyridine was added, the latter ones present an increase on the emission intensity and a reduction of FWHM. Thus, the additive enhanced the emission properties of $MAPbBr_3$, as expected, due to the fact that its incorporation suppresses the crystallographic defects and decreases the trap density. With less defects in its lattice, charges recombine less through defects and more radiatively, hence the emission intensity increase. Therefore, although films in which pyridine was added were not overall morphologically better, the incorporation of pyridine

helps improving perovskite structure, by reducing the density of trap defects. Moreover, as the films have similar thicknesses (422.5 ± 19.75 nm and 425 ± 21.01 nm for pristine and films prepared with pyridine, respectively), pyridine addition improved the structural quality of $MAPbBr_3$.

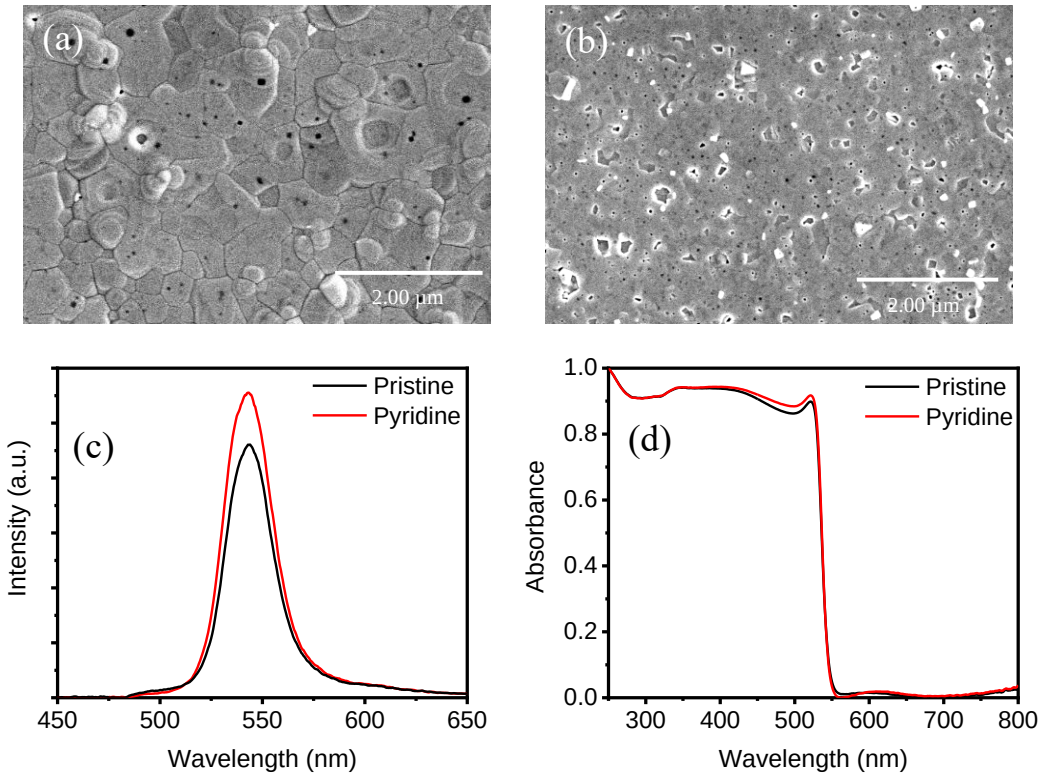

Figure 12. SEM images of a $MAPbBr_3$ pristine film (a) and a film fabricated with pyridine addition (b); PL (c) and absorbance spectra (d) of pristine films (black) and films fabricated with pyridine addition (red).

Concerning the absorbance spectrum displayed in Figure 12, it shows that films fabricated with the addition of pyridine have slightly stronger absorption between 521.5 nm, its absorption peak, and 347.5 nm of incoming light than pristine films. Although at around 500 nm there is a decrease in the irradiance from the sun, it is extremely important that the perovskite absorbs as much as possible from the solar spectrum, especially considering wide-bandgap solar cells. The addition of pyridine did not change the films' bandgap, both having a bandgap energy of 2.30 eV, as seen in appendix C Figure 27.

The PV performance of devices fabricated with both precursor solutions was also assessed, having the following structure: ITO/SnO_2/$MAPbBr_3$ (pyridine)/Spiro-MeOTAD/Au. According to the presented results and the literature, pyridine addition enhances the overall properties of $MAPbBr_3$ films, by improving its structural properties and reducing defects, so it would be expected that devices fabricated with pyridine would perform better than pristine ones. However, this did not happen, as the J-V plots presented in Figure 13, and the PV parameters in Table 4 show that the best pristine device achieved a PCE of 2.24 % (V_{OC} = 0.89 V, J_{SC} = 3.90 mA/cm^2, FF = 64.41 %), whereas the best device fabricated with pyridine achieved a PCE of only 1.57 % (V_{OC} = 0.93 V, J_{SC} = 2.63 mA/cm^2, FF = 63.94 %). Moreover, pristine devices achieved, on average, higher values for the PV parameters as seen in the box charts presented in appendix section D Figure 31. In addition, regardless of the pyridine concentration, the V_{OC} was low for all the devices, meaning that the synthesised $MAPbBr_3$ on SnO_2 was not good. The presence of pinholes can explain the lower J_{SC}, however their presence would also lead to lower shunt resistance decreasing the FF, which it is not the case. Air-processing of solar cells can explain the poor quality of the devices given the sensitivity of perovskite to ambient air.

Table 4. Photovoltaic parameters of pristine devices and devices fabricated with pyridine fabricated in ambient air.

Absorber layer	V_{OC} (V)	J_{SC} (mA/cm^2)	FF (%)	PCE (%)
$MAPbBr_3$	0.89	3.90	64.41	2.24
$MAPbBr_3$ with pyridine	0.93	2.63	63.94	1.57

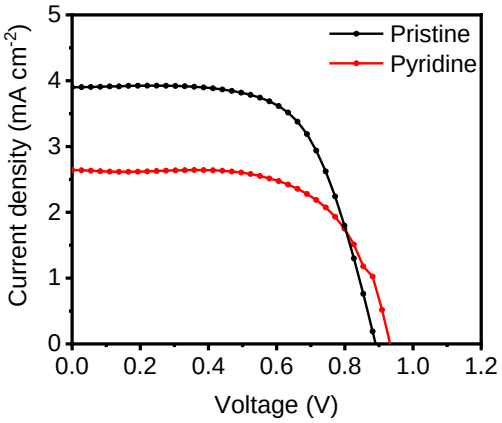

Figure 13. J-V curves of $MAPbBr_3$ pristine devices and devices fabricated with pyridine.

As the results were not satisfactory, the experiment was repeated, but results were very similar, as the devices fabricated with pyridine continued to underperform when compared with pristine devices. In addition, for both pristine and pyridine devices, V_{OC} continued to be low.

So, it was decided to fabricate the devices again, but this time the perovskite layer was deposited inside a GB where oxygen and humidity levels are well controlled by inert gas flow (N_2). The PV parameters of the best devices are presented in Table 5. This time it is clear to see the effect of the addition of pyridine in $MAPbBr_3$ films. On this batch, contrary to the previous, the positive effect of pyridine is confirmed, as pristine devices achieved a maximum PEC of 3.11 % (V_{OC} = 1.36 V, J_{SC} = 3.59 mA/cm^2, FF = 63.42 %), and devices fabricated with pyridine achieved a maximum PCE of 4.32 % (V_{OC} = 1.33 V, J_{SC} = 4.26 mA/cm^2, FF = 76.43 %). By adding pyridine to $MAPbBr_3$, it was possible to increase all the parameters, without exception. The box charts, displayed in section D Figure 32, show that the PCE efficiency in pyridine devices is higher. The controlled environment allowed the formation of higher quality $MAPbBr_3$ reducing the trap density and increasing V_{OC} and J_{SC}.

Table 5. Photovoltaic parameters of $MAPbBr_3$ pristine devices and devices fabricated with pyridine fabricated inside of a GB.

Active layer	V_{OC} (V)	J_{SC} (mA/cm$_2$)	FF (%)	PCE (%)
$MAPbBr_3$	1.37	3.59	63.42	3.12
$MAPbBr_3$ with pyridine	1.36	4.13	78.49	4.40

All in all, it was confirmed that pyridine is a compatible compound to be used as an additive as it enhances the perovskite performance and properties. The poorer surface coverage can possibly be explained by the fact that cells were air processed, since when they were deposited inside of the GB, cells with pyridine performed better than pristine devices. It was shown once again that the precise control of ambient conditions is extremely important when fabricating such sensitive materials.

3.2 QDs in Perovskite Matrix

After the development of the first $MAPbBr_3$ solar cells, devices fabricated via one-step with a 1.0 M precursor solution yielded the most efficient and stable cells, when compared with the two-step approach. Pyridine

addition in ambient air did not yield the expected enhancement of the devices, despite achieving good results when fabricated in controlled atmospheric conditions. After these steps, the stability of 1.0 M $MAPbBr_3$ films and devices fabricated via one -step was investigated.

In order to further enhance the stability of PSCs, PbS QDs can be added in small concentrations to the perovskite matrix, ranging from 0.2 mg/mL up to 5.0 mg/mL, as mentioned in the Introduction section 1.4.4.[44], [63] However, some recent literature has been exploring $MAPbBr_3$ and PbS-QDs concerning the development of IBSCs, which requires higher concentration of QDs, and, to our knowledge, there are no studies regarding its long-term stability enhancement. As such, the following sub-sections analyse the inclusion of QDs with different ranges of concentration in the perovskite host, in order to assess the long-term stability of devices both in vacuum and in ambient air conditions.

3.2.1 Low QDs Concentration

To study the influence of PbS-QDs in the perovskite matrix, 0.05 mg/mL of QDs were added into $MAPbBr_3$ precursor solution. Previous works [41], [46], [47] have shown that the QDs inclusion can aid the perovskite film nucleation, as they act as nucleation sites that promote the perovskite growth, thus improving the films' morphology regarding grain size, surface coverage and uniformity. Looking at the SEM images in Figure 14, the addition of low concentration of QDs did not improve surface coverage, since in pristine films it was already excellent. On the other hand, its addition, even though in really small concentration, was enough to slightly increase the grain size from 217.64 ± 58.18 nm to 235.33 ± 86.00 nm. To further assess the impact on morphology, atomic force microscopy (AFM) could be used to measure roughness and evaluate the films' uniformity. It is relevant to mention how much smaller the grains are and how much thinner (379.00 ± 30.65 nm and 374.00 ± 28.27 nm for pristine and $MAPbBr_3$/PbS QDs, respectively) the films are when compared with the 1.0 M films fabricated on the optimisation section (3.1.1.1Concentration Study). Higher ambient temperatures can explain smaller grain sizes as the antisolvent evaporates faster, but it cannot

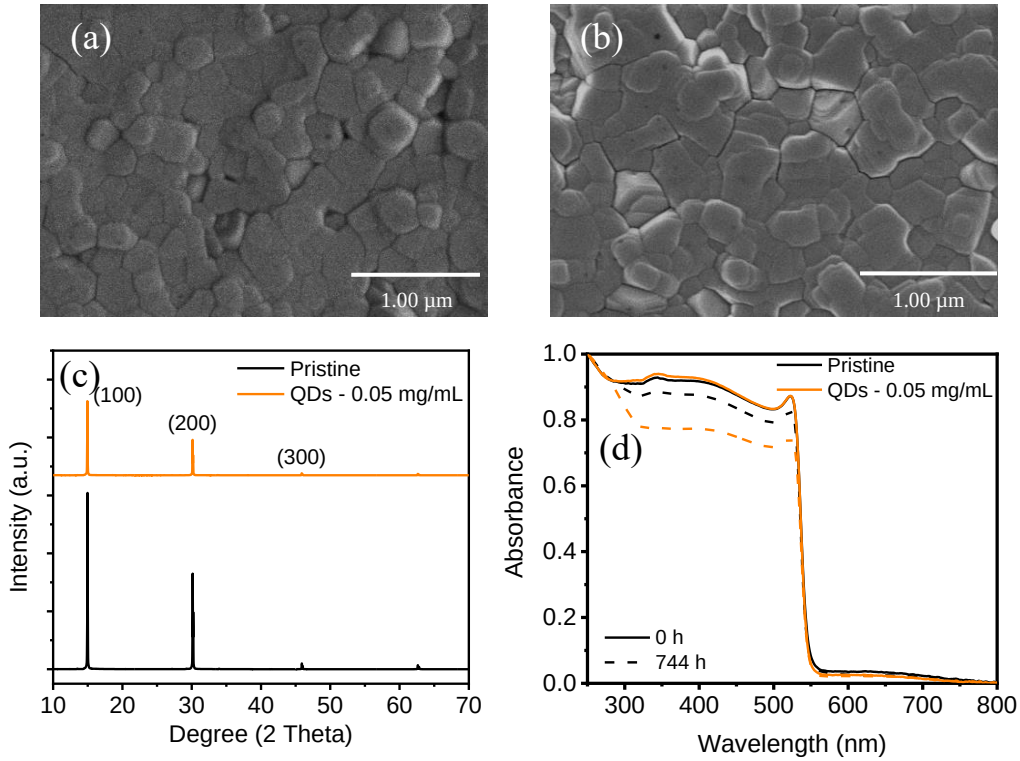

Figure 14. SEM images of $MAPbBr_3$ pristine films (a) and films synthesised with 0.05 mg/mL PbS QDs in perovskite matrix (b); XRD (c) and absorbance spectra (d) of films synthesised wit and without PbS QDs.

explain the synthesis of thinner films, as the thickness is primarily defined by the volume of the precursor solution used.

The XRD data confirms the formation of $MAPbBr_3$ as three main diffraction peaks can be seen at 14.96°, 30.14°, and at 45.89° in Figure 14, which correspond to (100), (200), and (300) planes of the $MAPbBr_3$'s cubic structure, respectively, and indicate the growth preference in the ⟨100⟩ direction. The peaks intensity reveal that pristine films have a more ordered crystalline structure. The lattice mismatch between the QDs and $MAPbBr_3$, which induces defects in the perovskite matrix, can be the reason why pristine films have higher crystallinity. This affects the PCE leading to its decrease.[64] Moreover, no diffraction peaks related to PbS-QDs were detected due to their small size and low concentration.

The introduction of QDs had no influence in the absorbance spectrum, so, on the first measurements at 0 h, the absorbance spectra overlap one another as seen in Figure 14. It would be expected that with the introduction of PbS QDs, films and devices would become more stable. However, this was not observed. On a second measurement, after being stored for 744 h in ambient air, even though both films show a decrease in absorbance, it is more pronounced for films embedded with QDs. Whereas pristine films managed to keep 95 % of their initial absorbance peak intensity, films with QDs only kept 85 %. Additionally, the incorporation of PbS-QDs did not change the bandgap energy of the films as seen in Figure 28.

To further assess the incorporation of PbS-QDs into the perovskite matrix, devices were fabricated with the following structure: ITO/c-TiO_2/m-TiO_2/$MAPbBr_3$ (PbS QDs)/Spiro-MeOTAD/Au. The J-V plot is presented in Figure 15, and the PV parameters in Table 6. As it was expected from the XRD analysis, the lower crystallinity of the films when QDs were incorporated resulted in lower PCE, as displayed in the box charts in appendix section D Figure 33. Pristine devices achieved a maximum PCE of 3.95 % (V_{OC} = 1.28 V, J_{SC} = 4.12 mA/cm^2, FF = 74.72 %), and devices with incorporated QDs achieved a maximum efficiency of only 2.88 % (V_{OC} = 1.19 V, J_{SC} = 3.47 mA/cm^2, FF = 69.65 %).

Table 6. Photovoltaic parameters of $MAPbBr_3$ pristine devices and devices fabricated with the inclusion of 0.05 mg/mL PbS QDs measured after fabrication. The percentual enhancements (gains) of each parameter due to the QDs inclusion are indicated in the bottom row.

PbS QDs concentration	V_{OC} (V) | Gain (%)	J_{SC} (mA/cm^2) | Gain (%)	FF (%) | Gain (%)	PCE (%) | Gain (%)
No QDs (pristine)	1.28	4.12	74.72	3.95
0.05 mg/mL	1.19 | −7.03	3.47 | −15.8	69.65 | −6.79	2.88 | −27.1

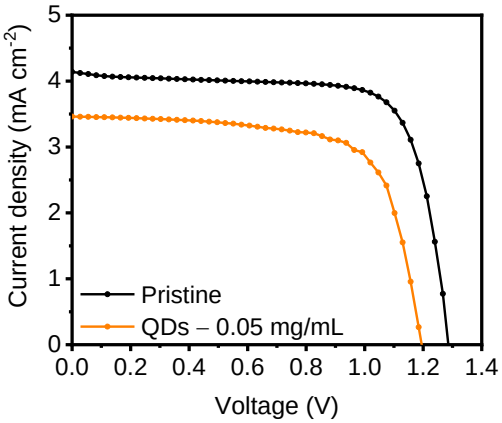

Figure 15. J-V curves of $MAPbBr_3$ pristine devices and devices fabricated with 0.05 mg/mL PbS QDs.

Regarding the stability of the devices, the PCE of four cells, two pristine (P1 and P2), and two fabricated with PbS QDs (Q1 and Q2), continued to be assessed, as displayed in Figure 16. For the first 576 h, the cells were kept under vacuum (desiccator) and hidden from light. From 576 h onward, two of the devices, one pristine (P2) and the other fabricated with PbS QDs (Q2), were kept in ambient air, but still in the dark.

Interestingly, when analysing the parameters, all devices show an increasing trend in V_{OC} overtime. It is stated that long-term storage of the devices in vacuum releases the stress caused by lattice distortion.[65] This leads to the raise in the diffraction peak intensity of perovskites suggesting the increase in grain size. Additionally, FWHM also decreases which can be explained by the increase of the perovskite crystallite size. All these factors, lead to an improvement in the perovskite's quality which results in V_{OC} increasement. Moreover, given the fact that they were kept under vacuum, possibly simulating the behaviour of encapsulated devices, J_{SC} stays constant during the first 576 h. If they were kept in ambient air, moisture and oxygen would lead to the degradation of the perovskite layer.[65] Consequently, its crystallinity would decrease causing the absorption of incident light to drop, which is exactly what happened to the synthesised films, as seen in Figure 14. After being stored 576 h in vacuum, P1 kept the same initial PCE (3.96 %), P2 increased it by 5 % (3.03 %), Q1 kept 94 % (2.88 %), and Q2 kept 97 % (2.43 %), as represented in Table 7.

Table 7. PCE measurements of $MAPbBr_3$ devices fabricated with and without 0.05 mg/mL PbS QDs over a period of 1113 h. Devices P1 and Q1 were always kept in vacuum, whereas devices P2 and Q2 after 576 h started being kept in ambient air.

Cell	QDs Concentration	PCE (%) at				
		0 h	576 h	744 h	912 h	1113 h
P1	No QDs (pristine)	3.95	3.96	3.83	3.52	3.19
P2	No QDs (pristine)	2.89	3.03	2.51	2.92	2.06
Q1	0.05 mg/mL	2.88	2.71	2.50	1.86	-
Q2	0.05 mg/mL	2.51	2.43	2.31	1.86	-

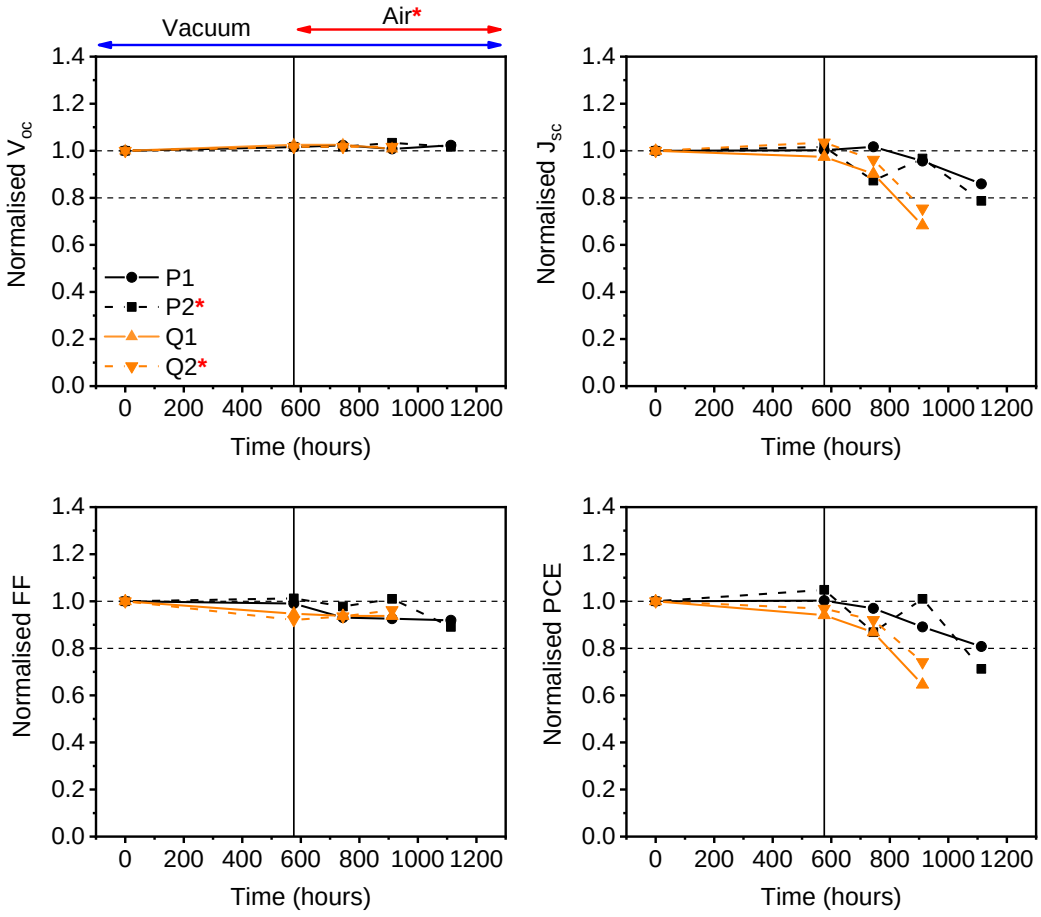

Figure 16. Photovoltaic parameters tracking of $MAPbBr_3$ devices fabricated with and without 0.05 mg/mL PbS QDs for over 1113 h. Devices P1 and Q1 were always kept in vacuum, whereas devices P2 and Q2 after 576 h started being kept in ambient air.

As P2 and Q2 are moved outside, they are exposed to oxygen and moisture, and, since J_{SC} is majorly influenced by the cells' absorption, a drop in photocurrent was expected. This is confirmed by a decreasing trend of PCE. Nevertheless, the decline is much sharper on cells fabricated with QDs, showing the poorer quality of such devices. Cells that were still being kept under vacuum also show a decrease in PCE. The drop can be explained by the fact during this time, when devices were measured, the RH was higher than usual (70-85 % compared to normal values of 55-65 %, during such time of the year), degrading not only P2 and Q2, but also P1 and Q1. From 912 h onward, cells fabricated with QDs fully stopped working, whereas pristine devices managed to continue operating. On the last measurement, 1113 h after being fabricated, P1 managed to keep 81 % (3.19 %) of its initial measured PCE and P2 retained 71 % (2.06 %), as seen in Table 7.

All in all, such low concentration of QDs is not enough to enhance the perovskite layer and improve its stability.

3.2.2 Moderate QDs Concentration

Since a low concentration of QDs did not improve the stability of $MAPbBr_3$ solar cells, a concentration on the other end of the spectrum, 5.00 mg/mL of PbS QDs was incorporated into the perovskite matrix.

For moderate QDs concentration, the SEM image in Figure 17 show an improvement in uniformity. When comparing the synthesised films with pervious pristine ones, 5.00 mg/mL films are more uniform. Since pristine films were already compact and presented good surface coverage, the addition of QDs in higher concentrations, just like in low concentration, did not improve those factors. Overall, increasing the concentration of QDs in the perovskite matrix improves the film's morphology, as it is more uniform.

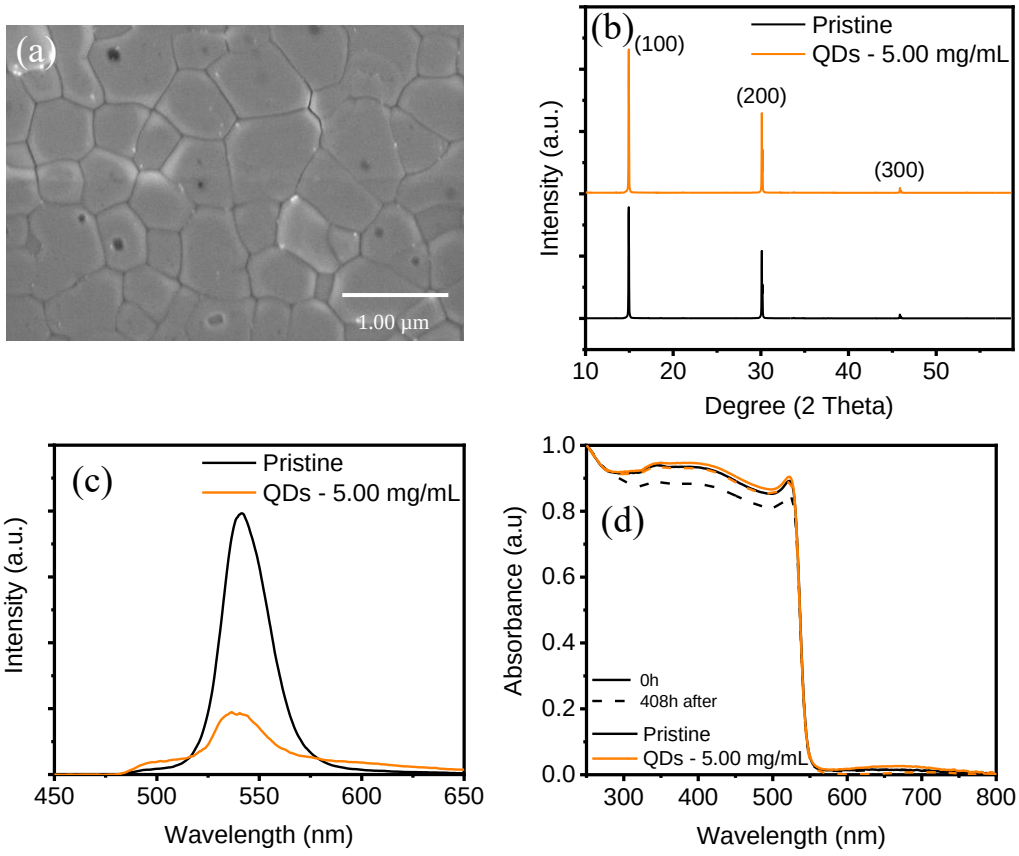

Figure 17. SEM image of a $MAPbBr_3$ film synthesised with 5.00 mg/mL PbS QDs in perovskite matrix (a); XRD (b), PL (c) and absorbance spectra (d) of films synthesised wit and without 5.00 mg/mL PbS QDs.

The XRD data confirms the formation of $MAPbBr_3$ as three main diffraction peaks can be seen at 14.93°, 30.10°, and at 45.86° in Figure 17, which correspond to (100), (200), and (300) planes of the $MAPbBr_3$'s cubic

structure, respectively, and indicate the growth preference in the ⟨100⟩ direction. Contrary to the results obtained on the previous section, the addition of QDs in high concentration resulted in films with higher crystallinity than pristine films. It may be contradictory since lattice mismatch would be more impactful as the concentration of QDs increases, but it was demonstrated in $MAPbI_3$ solar cells that by increasing the concentration of QDs the crystalline properties of the films improved, which led to higher PCE.[66] In addition, no diffraction peaks related to PbS-QDs were detected. Thus, increasing the concentration of QDs improved the structural properties of the perovskite layer, however it is something that we still cannot understand.

In the PL analysis, pristine films display a more intense emission peak than films prepared with QDs, as seen in Figure 17. The introduction of QDs, originated defects, therefore, charges will recombine through defect levels, which explains the lower emission peak intensity.

Regarding the optical properties of the films, similarly to the incorporation of QDs in low concentration, in an initial measurement, there is no major difference between the UV-Vis spectra of the films in Figure 17. Additionally, adding PbS-QDs in moderate concentration did not change the bandgap energy of $MAPbBr_3$ films, confirmed by the Tauc plot in appendix section C Figure 29. But, contrary to the incorporation of QDs in lower concentration, after 408 h of being stored in ambient air, films with PbS-QDs were able to keep almost the same absorbance curve, whereas pristine films show a noticeable decrease in absorbance. Pristine films kept 95 % of their initial absorbance and films with dots managed to maintain 99 %. This can be explained by the fact that with the introduction of PbS QDs halide vacancies and dangling bonds where occupied. Besides that, the Pb in PbS has a strong interaction with Br^- ions. All this together inhibits ion migration leading to an increase in stability. As there is nothing preventing the ion migration in pristine films, their degradation rate is much faster.

To further assess the incorporation of PbS QDs into the perovskite matrix, devices were fabricated with the following structure: ITO/c-TiO_2/m-TiO_2/$MAPbBr_3$ (PbS QDs)/Spiro-MeOTAD/Au. The J-V plot is presented in Figure 18, and the PV parameters in Table 8. In opposition to the PV results from devices with low concentration of QDs, as expected from XRD, 5.00 mg/mL devices achieved, on average, higher PCE than pristine ones (1.71 % and 1.78 % on average for pristine and QDs devices, respectively), as seen in box charts in appendix section D Figure 34. Pristine devices achieved a maximum PCE of 2.24 % (V_{OC} = 0.95 V, J_{SC} = 3.51 mA/cm^2, FF = 66.91 %), and devices with the inclusion of QDs achieved a maximum PCE of 2.30 % (V_{OC} = 1.21 V, J_{SC} = 2.88 mA/cm^2, FF = 66.97 %). When comparing these results with the ones obtained from devices fabricated with low concentration of QDs, cells perform on average worse. This happens since the devices were air-processed, which makes reproducibility much harder.

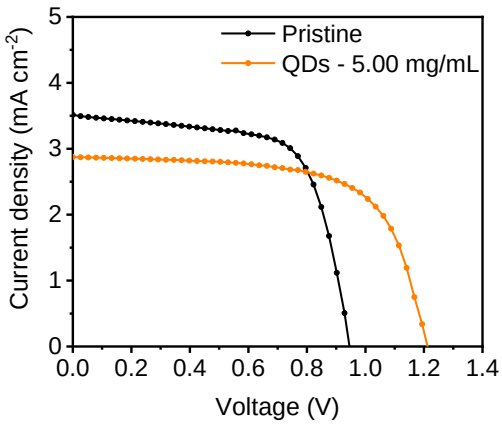

Figure 18. J-V curves of pristine $MAPbBr_3$ devices and devices fabricated with the inclusion of 5.00 mg/mL PbS-QDs.

Table 8. Photovoltaic parameters of $MAPbBr_3$ pristine devices and devices fabricated with the inclusion of 5.00 mg/mL PbS QDs measured after fabrication. The percentual enhancements (gains) of each parameter due to the QDs inclusion are indicated in the bottom row.

PbS QDs concentration	V_{OC} (V) | Gain (%)	J_{SC} (mA/cm^2) | Gain (%)	FF (%) | Gain (%)	PCE (%) | Gain (%)
No QDs (pristine)	0.95	3.51	66.91	2.24
5.00 mg/mL	1.21 | 27.4	2.88 | −17.9	65.97 | −1.40	2.30 | 2.68

Regarding the stability of the devices, the maximum power point of four devices, two pristine (P3 and P4) and two fabricated with the inclusion of 5.00 mg/mL PbS QDs (Q3 and Q4), continued to be assessed, as displayed in Figure 19. For the first 1968 h they were kept under vacuum (desiccator) and hidden from light. From 1968 h onward, two of the devices, one pristine (P4) and the other fabricated with PbS QDs (Q4), were kept in ambient air, but still in the dark.

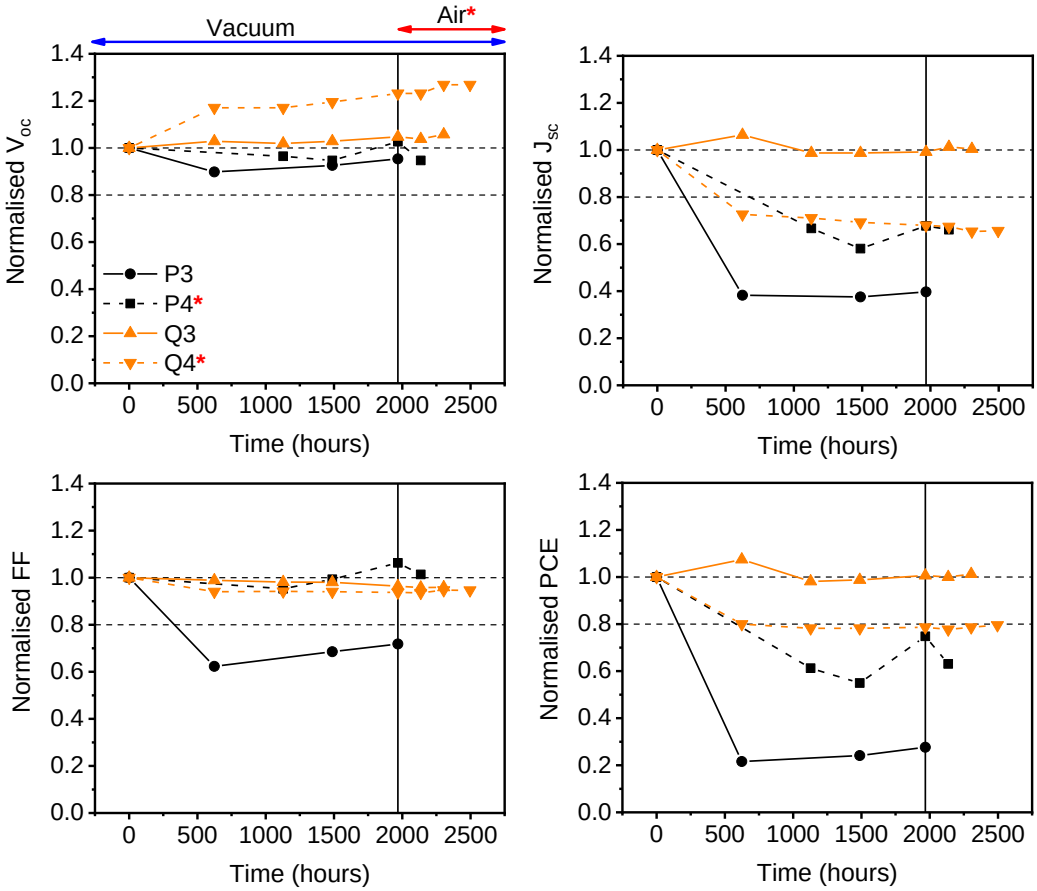

Figure 19. Photovoltaic parameters tracking of $MAPbBr_3$ devices fabricated with and without 5.00 mg/mL PbS QDs for over 2496 h. Devices P3 and Q3 were always kept in vacuum, whereas devices P4 and Q4 after 576 h started being kept in ambient air.

Table 9. PCE measurements of $MAPbBr_3$ devices fabricated with and without 5.00 mg/mL PbS QDs over a period of 2496 h. Devices P3 and Q3 were always kept in vacuum, whereas devices P4 and Q4 after 1968 h started being kept in ambient air.

Cell	QDs Concentration	PCE (%) at 0 h	624 h	1128 h	1488 h	1968 h	2136 h	2304 h	2496 h
P3	No QDs (pristine)	1.99	0.43	-	0.48	0.55	-	-	-
P4	No QDs (pristine)	1.11	-	0.68	0.61	0.83	0.70	-	-
Q3	5.00 mg/mL	1.61	1.73	1.58	1.59	1.62	1.61	1.63	-
Q4	5.00 mg/mL	2.20	1.76	1.72	1.72	1.73	1.71	1.73	1.75

During the first 624 h, the V_{OC} of devices fabricated with QDs follows an increasing trend, which can be explained by the age-induced recrystallisation. However, Q4 shows a decrease in J_{SC} which results in a decline of its PCE. Air-processing of perovskites is a challenging procedure, and, therefore, reproducibility is harder to achieve. This leads to PSCs with different quality, possibly explaining the dissimilar rates of degradation of devices fabricated with the incorporation of QDs. Moreover, this also detected in pristine devices, where a drop in all parameters is observed, result of an initial degradation. However, the greater degradation is possibly due to their higher sensitivity. For the rest of the period in vacuum, no more significant changes are observed ,with the exception of P4 that had high variations. So, after 1968 h, P3 kept only 28 % (0.55 %) of its initial PCE, P4 kept 75 % (0.83 %), Q3 increased it by 1 % (1.62 %), and Q4 kept 79 % (1.62 %) (99 % if considering the starting point at 624 h), as seen in Figure 19.

As soon as the devices P4 and Q4 were kept outside, at the moment when RH increased, pristine devices started to degrade, whereas cells fabricated with QDs managed to keep its consistency. On the other hand, P3 stopped working instantly, and P4's PCE declined with a sharp slope, eventually stopping working. The pristine devices stopped working sooner than the pristine ones fabricated on the low PbS QDs concentration study, because on this batch they had lower quality. Nevertheless, in both studies, pristine devices degrade when exposed to harsher conditions. On the last measurement, as Q3's contact was worn out thus, it was not possible to get its J-V curve. Nevertheless, it is expected that its parameters would remain constant, as after 2304 h its PCE was 1 % higher (1.63 %) than its first value as seen in Table 9, indicating excellent stability. Regarding Q4, despite being stored in ambient air, it managed to keep its PCE the same as when it was stored in vacuum, despite an initial drop in the first 624 h, which shows that the incorporation of QDs in the perovskite matrix prevents the gradation of PSCs. After 2496 h, Q4's PCE was 80 % (1.75 %) of its initial value, and 99 % considering the starting point at 624 h.

On the whole, with higher concentrations of PbS QDs, it is possible to increase PSCs' stability.

3.2.3 Multiple QDs concentrations

After the previous results, it was proven that the increase in concentration of QDs improves the films' morphology and structural properties, leading to higher stability. So, in order to better understand the influence of the concentrations of QDs in the stability of devices, multiple concentrations of PbS-QDs in perovskite matrix were tested. For this, 0.50 mg/mL, 1.00 mg/mL, 2.00 mg/mL, and 5.00 mg/mL PbS QDs were incorporated in the perovskite matrix.

Different PbS-QDs concentrations synthesised films with different thicknesses (pristine, 0.50 mg/mL, 1.00 mg/mL, 2.00 mg/mL, and 5.00 mg/mL films have on average a thickness of 342.00 ± 22.65 nm, 327.00 ± 10.55 nm, 337.00 ± 4.83 nm, 357.50 ± 24.41 nm, and 371.00 ± 2.94 nm, respectively), and, looking

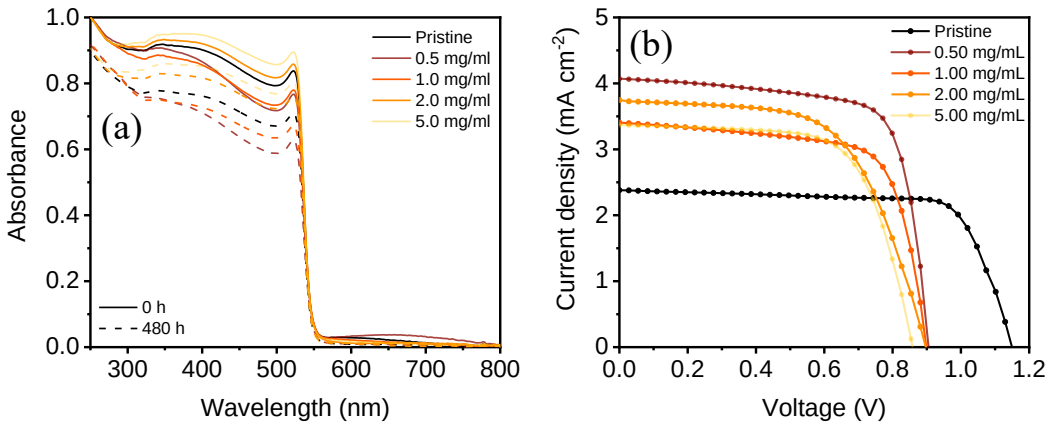

Figure 20. PL Absorbance spectra of synthesised $MAPbBr_3$ pristine films and films with the inclusion of 0.50 mg/mL, 1.00 mg/mL, 2.00 mg/mL, and 5.00 mg/mL PbS QDs (a); J-V of fabricated $MAPbBr_3$ and $MAPbBr_3$ with PbS-QDs devices (b)

at the UV-Vis spectra in Figure 20, thicker films absorbed more of the incoming light. When comparing the optical stability of the films after 480 h stored in ambient air, high concentrations of QDs help retarding the degradation, whereas low concentration does not. After this period, the absorption peak of pristine films was 85 % as intense as the initial, whereas for 0.50 mg/mL films it was only 82 %. On the other hand, as concentration increases, films retained more of their initial absorbance, as 1.00 mg/mL, 2.00 mg/mL, and 5.00 mg/mL films' absorbance peaks were 86 %, 89 % and 90 % as intense as the initial peak.

To further assess the incorporation of PbS QDs into the perovskite matrix, devices were fabricated with the following structure: ITO/c-TiO_2/m-TiO_2/$MAPbBr_3$ (PbS QDs)/Spiro-MeOTAD/Au. The J-V plot is presented in Figure 20, the PV parameters in Table 10, and box charts in the appendix section D Figure 35. Devices fabricated with the addition of 0.50 mg/mL QDs, achieved the highest PCE of all the devices, converting 2.68 % of the incident power (V_{OC} = 0.91 V, J_{SC} = 4.07 mA/cm^2, FF = 72.79 %). It was followed by 1.00 mg/mL films which achieved a maximum PCE of 2.15 % (V_{OC} = 0.90 V, J_{SC} = 3.41 mA/cm^2, FF = 70.22 %), then by pristine devices which achieved a maximum PCE of 2.07 % (V_{OC} = 1.15 V, J_{SC} = 2.38 mA/cm^2, FF = 75.73 %), and by 2.00 mg/ml cells achieving a maximum PCE of 2.03 % (V_{OC} = 0.90 V, J_{SC} = 3.74 mA/cm^2, FF = 60.60 %). In last, 5.00 mg/mL devices were the least efficient with maximum PCE of only 1.94 % (V_{OC} = 0.86 V, J_{SC} = 3.37 mA/cm^2, FF = 67.14 %). During the deposition of the perovskite layers, air temperature was high (25 °C) which makes the depositions more challenging, resulting in cells with low V_{OC}, as demonstrated in previous sections.

Table 10. Photovoltaic parameters of $MAPbBr_3$ pristine devices and devices fabricated with different concentrations of PbS QDs measured after fabrication.

PbS QDs concentration	V_{OC} (V) | Gain (%)	J_{SC} (mA/cm^2) | Gain (%)	FF (%) | Gain (%)	PCE (%) | Gain (%)
No QDs (pristine)	1.15	2.38	75.73	2.07
0.50 mg/mL	0.91 | −20.9	4.07 | 71.0	72.79 | −3.88	2.68 | 29.5
1.00 mg/mL	0.90 | −21.7	3.41 | 43.3	70.22 | −7.28	2.15 | 3.86
2.00 mg/mL	0.90 | −21.7	3.74 | 57.1	60.60 | −20.0	2.03 | −1.93
5.00 mg/mL	0.86 | −25.2	3.37 | 41.6	67.14 | −11.3	1.94 | −6.28

Regarding the stability of the devices, the maximum power point of ten devices, two pristine (P5 and P6), two fabricated with the incorporation of 0.50 mg/mL QDs (Q5 and Q6), two fabricated with the incorporation of 1.00 mg/mL QDs (Q7 and Q8), two fabricated with the incorporation of 2.00 mg/mL QDs (Q9 and Q10) and two fabricated with the incorporation of 5.00 mg/mL QDs (Q11 and Q12), continued to be assessed, as seen in Figure 21. For the first 1320 h they were kept under vacuum (desiccator) and hidden from light. From 1320 h onward, five of the devices, one pristine (P6) and four others fabricated with PbS QDs (Q6, Q8, Q10, and Q12), were kept in ambient air, but still hidden from light.

During the first 408 h, the V_{OC} of devices fabricated with greater concentration of QDs, 2.00 mg/mL and 5.00 mg/mL, shows an increase trend, explained by age-induced recrystallisation, leading to a PCE increase of more than 10 %, as seen in Figure 21 and Table 11. Although cells fabricated with other concentrations maintain or also increase their V_{OC} during this period, a drop in J_{SC}, due to their poorer quality, causes their PCE to decrease, being this effect more pronounced in pristine devices P5 and P6. For the rest of the time until 1320 h, no significant changes are seen, and devices keep their PCE values. After 1320 h, P5 kept 52 % of its initial PCE value, P6 kept 51 %, Q5 kept 74 %, Q5 kept 99 %, Q7 kept 84 %, Q8 kept 91 %, Q9 kept 83 %, Q10 increased it by 18 %, Q11 kept 93 %, and Q12 also increased it by 9 %. So, it is clear to see that the incorporation of QDs, even when in vacuum, helps retarding the devices' degradation.

Just like in the two previous studies, when P6, Q6, Q8, Q10 and Q12 started being stored in ambient air, the RH increased. After that point, pristine devices were majorly affected by moisture and oxygen, as both stopped working shortly after, which, once again demonstrates how sensitive perovskite materials are. The rest of the cells, also show a decreasing trend, but at much slower rate. Regarding 0.50 mg/mL cells, even though they worked longer than pristine ones, it's clear to see that they show a shaper decline than the other cells with higher concentration of QDs, with Q6 stopping performing 168 h after continuous exposure to ambient air. Q8, another device stored in ambient air, fabricated with 1.00 mg/mL, stopped performing at the exact same time. From 0.50 mg/mL and 1.00 mg/mL devices, only the ones that remained in vacuum managed to keep functioning, but still being possible to be observed a decline trend in PCE. However, for higher QDs' concentration, devices' degradation is not as significant. Even though Q10, which started being stored in ambient air, shows a decrease in J_{SC}, it has little impact in PCE as the decline trend presets a small slope. Device Q12 fabricated with 5.00 mg/mL, shows a higher degradation rate, but after 1776 h it still maintained more than 90 % of its initial PCE value. Nevertheless, it was proven when studying the incorporation of QDs in high concentration, that 5.00 mg/mL devices are able to keep their PCE even after of being exposed to ambient air in Figure 19. On the last measurement Q5 kept 48 % (0.98 %) of its initial PCE, Q7 kept 71 % (1.43 %), Q9 kept 71 % (1.37 %), Q10 increased it by 12 % (2.28 %), Q11 kept 89 % (1.60 %), and Q12 kept 94 % (1.69 %), as seen in Table 11. All in all, as the concentration of QDs in the perovskite matrix increases, devices' stability is enhanced.

Table 11. PCE measurements of $MAPbBr_3$ devices fabricated with and without 0.05 mg/mL PbS QDs over a period of 1776 h. Devices P5, Q5, Q7, Q9 and Q11 were always kept in vacuum, whereas devices P6, Q6, Q8, Q10 and Q12 after 1320 h started being kept in ambient air.

Cell	QDs Concentration	PCE (%) at						
		0 h	408 h	648 h	840 h	1320 h	1488 h	1776 h
P5	No QDs (pristine)	2.07	-	-	1.03	1.08	-	-
P6	No QDs (pristine)	1.24	0.75	0.71	0.62	0.63	0.72	-
Q5	0.50 mg/mL	2.03	1.63	1.50	1.51	1.51	1.54	0.98
Q6	0.50 mg/mL	2.68	2.63	2.60	2.55	2.66	2.60	-
Q7	1.00 mg/mL	2.00	1.64	1.74	-	1.68	1.50	1.43
Q8	1.00 mg/mL	1.92	1.59	1.74	1.75	1.74	1.74	-
Q9	2.00 mg/mL	1.93	1.70	1.58	1.62	1.61	1.63	1.37
Q10	2.00 mg/mL	2.03	2.27	2.24	2.37	2.39	2.36	2.28
Q11	5.00 mg/mL	1.79	1.84	1.77	1.72	1.67	1.61	1.60
Q12	5.00 mg/mL	1.80	2.01	1.98	1.98	1.97	1.90	1.69

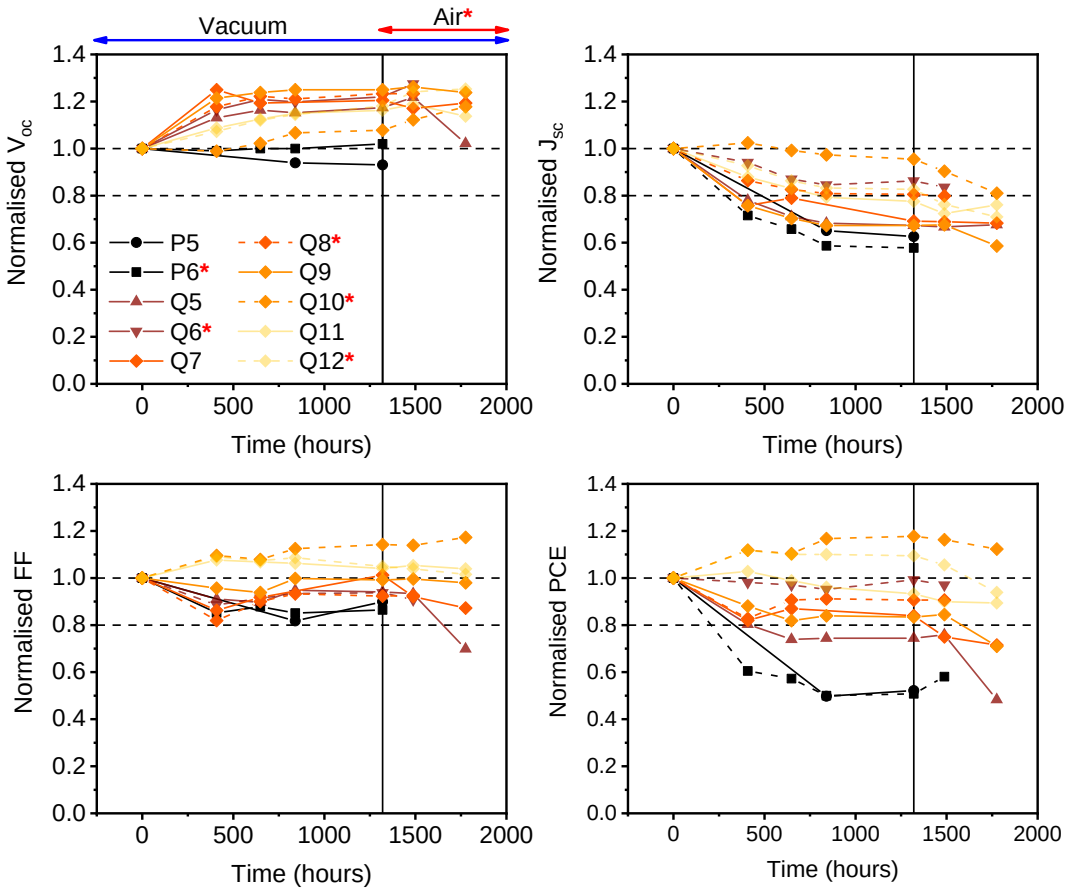

Figure 21. Photovoltaic parameters tracking of $MAPbBr_3$ devices fabricated with and without the inclusion of 0.50 mg/mL, 1.00 mg/mL, 2.00 mg/mL, and 5.00 mg/mL PbS-QDs for over 1776 h. Devices P5, Q5, Q7, Q9 and Q11 were always kept in vacuum, whereas devices P6, Q6, Q8, Q10 and Q12 after 1320 h started being kept in ambient air.

4

CONCLUSIONS

The main objective of this thesis was to improve the long-term stability of perovskite devices fabricated in ambient air, namely $MAPbBr_3$ solar cells. To further enhance the stability, PbS -QDs were incorporated into the perovskite's matrix. Additionally, pyridine was also subjected to study in order to improve the PSCs' performance.

On the first section of the thesis, films and devices fabricated via one-step and two-step deposition methods were developed. For the one-step approach, 1.0 M precursor solutions synthesised compact pinhole-free films, which had low density of trap defects, and, given their higher thickness when compared with 0.6 M and 0.8 M films, showed greater absorbance. Regarding the precursor solution solvent ratio study, DMF/DMSO 7:3 precursor solution produced thicker films, leading to higher absorbance, and the most efficient device, however DMF/DMSO 9:1 cells had on average higher PCE values. Not only that, but the latter ratio fabricated devices which parameters presented a smaller deviation, which is desired, especially in not controlled environments.

Regarding the two-step approach, the concentration of the precursor solutions (with 1:1, $PbBr_2$:MABr) ratio was initially studied. All the synthesised films with 1:1 ratio precursor solution presented poor surface coverage, and bad structural and optical properties. Therefore, 1:0.27 ratio was studied, and the quality of the films was enhanced significantly. The surface coverage was improved, and the absorbance also increased, considerably.

Despite the improvement in films synthesised via two-step, when one-step and two-step devices' performance was compared, one-step produced more efficient and stable devices. Although for both types of devices a decrease in FF was observed, due to perovskite degradation, it was much more severe on two-step solar cells.

With the addition of pyridine, the PCE was expected to improve from the suppression of structural defects. However, when fabricated in ambient air, pristine devices performed better than cells with pyridine. Nevertheless, when the depositions were done in a controlled environment, inside of the GB, the positive impact of pyridine was stated, as cells with pyridine obtained a PCE of 4.40%, whereas pristine devices could only reach a maximum of 3.12%.

Concerning the degradation of perovskites, the gradual increase in the concentration of PbS-QDs enhanced the overall properties of films and devices, resulting, ultimately, on the increase in long-term stability. On average, apart from an initial drop, all the devices maintained their PCE when kept in vacuum, which, in a way, simulate the behaviour of encapsulated devices. When it comes to the concentration, a very low one, 0.05 mg/mL, proved to be detrimental to the stability, as even when compared to pristine devices, their degradation rate was faster, especially when exposed to ambient air, becoming inoperable soon after. On the other hand, high concentrations, 2.00 mg/mL, and 5.00 mg/mL, demonstrated to be very stable, even when exposed

to moisture and oxygen, being capable to keep more than 80 % of their initial PCE in such conditions. Devices with these concentrations, when in vacuum for 1320 h, increased their PCE by 18 %, from 2.03 % to 2.39 %, and by 9 %, from 1.80 5 to 1.97 %, respectively, mainly due to a rise in V_{OC}, explained by age-induced recrystallisation. The exposure to ambient air led to a drop in J_{SC} resulting a decline of PCE on all devices, but 2.00 mg/mL solar cell still retained more than 12 % of its initial PCE value, this is 2.28 %, and 5.00 mg/mL maintained 94% of it, which corresponds to a PCE of 1.69 %.

Additionally, the results obtained in the QDs in Perovskite Matrix section are promising, not only for stability related studies, but also for IBSC investigation.

In summary, following a series of development steps and diverse deposition approaches, we have successfully achieved the fabrication of perovskite layers with good quality that, when in devices, exhibit compatible performance and stability with the findings reported in literature, with the addition that, in our study, $MAPbBr_3$ was fabricated in ambient air, and PbS-QDs were added to its matrix to enhance the stability, which, to our knowledge, has never been reported.

4.1 Future Perspectives

In order to further complement this study, a better optimisation of the deposition of $MAPbBr_3$, via one-step and two-step, should be carried out in ambient air conditions, so that films with better structural and optical properties are obtained, permitting the achievement of higher PCE values. Moreover, optimising the addition of pyridine in ambient air is also essential, as it was proven to enhance the quality of the perovskite layer. After optimising the depositions, the same studies conducted in this work regarding the introduction of PbS-QDs QDs could also be conducted but this time on solar cells with the active layer composed of $MAPbBr_3$ with pyridine an additive.

Additionally, QDs could also be added to the interfaces between $MAPbBr_3$, and the charge transporting layers to form passivation layers and further improve the stability, as it would prevent ion migration in sensitive regions of the cells. Not only that, but, apart from moisture and oxygen, other factors that shorten PSCs lifetime should also be studied, particularly heat, since when exposed to light devices heat up inevitably, fastening the degradation process. Studies regarding IBSC can also be done given the good PV performances of the cells fabricated in this thesis.

To increase the stability of MAPbBr3 solar cells even further, replacing the back contact or the HTL and the back contact with a carbon paste layer can also be done, as in the case of Spiro-MeOTAD, it forms a weak barrier for the diffusion of gold atoms that promote the degradation of perovskites. [18] At the same time, the replacement would allow the fabrication of large-scale production of PSCs, which is essential for the commercialisation of PSCs.

Another viable option after optimisation, is the integration of a $MAPbBr_3$ layer on triple junction tandem solar cells when coupled with perovskite (lower bandgap) and silicon solar cells, leading to an improvement in PCE.

BIBLIOGRAPHY

[1] G. Xie *et al.*, "Investigation on significant efficiency enhancement of thin crystalline silicon solar cells," *J. Photonics Energy*, vol. 13, no. 03, Sep. 2023, doi: 10.1117/1.JPE.13.035501.

[2] "Best Research-Cell Efficiencies Chart." https://www.nrel.gov/pv/assets/pdfs/best-research-cell-efficiencies.pdf (accessed Sep. 14, 2023).

[3] G. Niu, X. Guo, and L. Wang, "Review of recent progress in chemical stability of perovskite solar cells," *J. Mater. Chem. A*, vol. 3, no. 17, pp. 8970–8980, 2015, doi: 10.1039/c4ta04994b.

[4] T. A. Berhe *et al.*, "Organometal halide perovskite solar cells: Degradation and stability," *Energy Environ. Sci.*, vol. 9, no. 2, pp. 323–356, 2016, doi: 10.1039/c5ee02733k.

[5] M. Grätzel, "The light and shade of perovskite solar cells," *Nat. Mater.*, vol. 13, no. 9, pp. 838–842, Sep. 2014, doi: 10.1038/nmat4065.

[6] M. A. Green, A. Ho-Baillie, and H. J. Snaith, "The emergence of perovskite solar cells," *Nat. Photonics*, vol. 8, no. 7, pp. 506–514, Jul. 2014, doi: 10.1038/nphoton.2014.134.

[7] A. Kojima, K. Teshima, Y. Shirai, and T. Miyasaka, "Organometal halide perovskites as visible-light sensitizers for photovoltaic cells," *J. Am. Chem. Soc.*, vol. 131, no. 17, pp. 6050–6051, 2009, doi: 10.1021/ja809598r.

[8] T. Bin Song *et al.*, "Perovskite solar cells: Film formation and properties," *J. Mater. Chem. A*, vol. 3, no. 17, pp. 9032–9050, 2015, doi: 10.1039/c4ta05246c.

[9] J. H. Noh, S. H. Im, J. H. Heo, T. N. Mandal, and S. Il Seok, "Chemical management for colorful, efficient, and stable inorganic-organic hybrid nanostructured solar cells," *Nano Lett.*, vol. 13, no. 4, pp. 1764–1769, 2013, doi: 10.1021/nl400349b.

[10] A. W. Y. Ho-Baillie, J. Zheng, M. A. Mahmud, F.-J. Ma, D. R. McKenzie, and M. A. Green, "Recent progress and future prospects of perovskite tandem solar cells," *Appl. Phys. Rev.*, vol. 8, no. 4, Dec. 2021, doi: 10.1063/5.0061483.

[11] J. H. Montoya, L. C. Seitz, P. Chakthranont, A. Vojvodic, T. F. Jaramillo, and J. K. Nørskov, "Materials for solar fuels and chemicals," *Nat. Mater.*, vol. 16, no. 1, pp. 70–81, Jan. 2017, doi: 10.1038/nmat4778.

[12] I. Ramiro and A. Martí, "Intermediate band solar cells: Present and future," *Prog. Photovoltaics Res. Appl.*, vol. 29, no. 7, pp. 705–713, Jul. 2021, doi: 10.1002/pip.3351.

[13] A. Luque and A. Martí, "Increasing the Efficiency of Ideal Solar Cells by Photon Induced Transitions at Intermediate Levels," *Phys. Rev. Lett.*, vol. 78, no. 26, pp. 5014–5017, Jun. 1997, doi: 10.1103/PhysRevLett.78.5014.

[14] J. H. Noh, S. H. Im, J. H. Heo, T. N. Mandal, and S. Il Seok, "Chemical Management for Colorful, Efficient, and Stable Inorganic–Organic Hybrid Nanostructured Solar Cells," *Nano Lett.*, vol. 13, no. 4, pp. 1764–1769, Apr. 2013, doi: 10.1021/nl400349b.

[15] F. Di Giacomo, A. Fakharuddin, R. Jose, and T. M. Brown, "Progress, challenges and perspectives in flexible perovskite solar cells," *Energy Environ. Sci.*, vol. 9, no. 10, pp. 3007–3035, 2016, doi: 10.1039/C6EE01137C.

[16] K. Wojciechowski and D. Forgács, "Commercial Applications of Indoor Photovoltaics Based on Flexible Perovskite Solar Cells," *ACS Energy Lett.*, vol. 7, no. 10, pp. 3729–3733, Oct. 2022, doi: 10.1021/acsenergylett.2c01976.

[17] C. Zuo, H. J. Bolink, H. Han, J. Huang, D. Cahen, and L. Ding, "Advances in perovskite solar cells," *Adv. Sci.*, vol. 3, no. 7, pp. 1–16, 2016, doi: 10.1002/advs.201500324.

[18] C. Teixeira *et al.*, "Charge Extraction in Flexible Perovskite Solar Cell Architectures for Indoor Applications – with up to 31% Efficiency," *Adv. Funct. Mater.*, vol. 32, no. 40, p. 2206761, Oct. 2022, doi: 10.1002/adfm.202206761.

[19] Z. Wang, X. Zhu, J. Feng, D. Yang, and S. (Frank) Liu, "Semitransparent Flexible Perovskite Solar Cells for Potential Greenhouse Applications," *Sol. RRL*, vol. 5, no. 8, p. 2100264, Aug. 2021, doi: 10.1002/solr.202100264.

[20] T. Chen, J. Xie, and P. Gao, "Ultraviolet Photocatalytic Degradation of Perovskite Solar Cells: Progress, Challenges, and Strategies," *Adv. Energy Sustain. Res.*, vol. 3, no. 6, p. 2100218, Jun. 2022, doi: 10.1002/aesr.202100218.

[21] L. Fan, Z. Pei, P. Wang, and Z. Zheng, "Research Progress on the Stability of Organic–Inorganic Halide Perovskite Photodetectors in a Humid Environment Through the Modification of Perovskite Layers," *J. Electron. Mater.*, vol. 51, no. 6, pp. 2801–2818, Jun. 2022, doi: 10.1007/s11664-022-09548-0.

[22] M. Shirayama *et al.*, "Degradation mechanism of CH3NH3PbI3 perovskite materials upon exposure to humid air," *J. Appl. Phys.*, vol. 119, no. 11, Mar. 2016, doi: 10.1063/1.4943638.

[23] Y. Nakamura, N. Shibayama, K. Fujiwara, T. Koganezawa, and T. Miyasaka, "Degradation Mechanism of Halide Perovskite Crystals under Concurrent Light and Humidity Exposure," *ACS Mater. Lett.*, vol. 4, no. 12, pp. 2409–2414, Dec. 2022, doi: 10.1021/acsmaterialslett.2c00744.

[24] P. Tolueinia, H. Khassaf, A. Shirazi Amin, Z. M. Tobin, S. P. Alpay, and S. L. Suib, "Moisture-Induced Structural Degradation in Methylammonium Lead Iodide Perovskite Thin Films," *ACS Appl. Energy Mater.*, vol. 3, no. 9, pp. 8240–8248, Sep. 2020, doi: 10.1021/acsaem.0c00638.

[25] B. Kammlander *et al.*, "Thermal degradation of lead halide perovskite surfaces," *Chem. Commun.*, vol. 58, no. 97, pp. 13523–13526, 2022, doi: 10.1039/D2CC04867A.

[26] Z. Ahmad *et al.*, "Degradation analysis in mixed (MAPbI3 and MAPbBr3) perovskite solar cells under thermal stress," *J. Mater. Sci. Mater. Electron.*, vol. 30, no. 2, pp. 1354–1359, 2019, doi: 10.1007/s10854-018-0403-4.

[27] Q. Wali, F. J. Iftikhar, M. E. Khan, A. Ullah, Y. Iqbal, and R. Jose, "Advances in stability of perovskite solar cells," *Org. Electron.*, vol. 78, p. 105590, Mar. 2020, doi: 10.1016/j.orgel.2019.105590.

[28] H. Cho, J. S. Kim, Y.-H. Kim, and T.-W. Lee, "Influence of A-site cation on the thermal stability of metal halide perovskite polycrystalline films," *J. Inf. Disp.*, vol. 19, no. 1, pp. 53–60, Jan. 2018, doi: 10.1080/15980316.2018.1424652.

[29] H. Zheng *et al.*, "The influence of perovskite layer and hole transport material on the temperature stability about perovskite solar cells," *Sol. Energy*, vol. 159, no. September 2017, pp. 914–919, 2018, doi: 10.1016/j.solener.2017.09.039.

[30] M. Wang *et al.*, "Ultraviolet Filtration Passivator for Stable High-Efficiency Perovskite Solar Cells," *ACS Appl. Mater. Interfaces*, vol. 14, no. 17, pp. 19459–19468, May 2022, doi: 10.1021/acsami.2c01749.

[31] Y. Sun *et al.*, "Enhanced UV-light stability of organometal halide perovskite solar cells with interface modification and a UV absorption layer," *J. Mater. Chem. C*, vol. 5, no. 34, pp. 8682–8687, 2017, doi: 10.1039/C7TC02603J.

[32] P. Chen *et al.*, "Luminescent europium-doped titania for efficiency and UV-stability enhancement of planar perovskite solar cells," *Nano Energy*, vol. 69, p. 104392, Mar. 2020, doi: 10.1016/j.nanoen.2019.104392.

[33] J. Zhu *et al.*, "Ultraviolet filtration and defect passivation for efficient and photostable CsPbBr3

perovskite solar cells by interface engineering with ultraviolet absorber," *Chem. Eng. J.*, vol. 404, p. 126548, Jan. 2021, doi: 10.1016/j.cej.2020.126548.

[34] S. Ma, G. Yuan, Y. Zhang, N. Yang, Y. Li, and Q. Chen, "Development of encapsulation strategies towards the commercialization of perovskite solar cells," *Energy Environ. Sci.*, vol. 15, no. 1, pp. 13–55, 2022, doi: 10.1039/D1EE02882K.

[35] F. J. Aparicio *et al.*, "Enhancing Moisture and Water Resistance in Perovskite Solar Cells by Encapsulation with Ultrathin Plasma Polymers," 2018, doi: 10.1021/acsami.7b17824.

[36] C. C. Boyd, R. Cheacharoen, T. Leijtens, and M. D. McGehee, "Understanding Degradation Mechanisms and Improving Stability of Perovskite Photovoltaics," *Chem. Rev.*, vol. 119, no. 5, pp. 3418–3451, Mar. 2019, doi: 10.1021/acs.chemrev.8b00336.

[37] L. McGovern, M. H. Futscher, L. A. Muscarella, and B. Ehrler, "Understanding the Stability of MAPbBr 3 versus MAPbI 3 : Suppression of Methylammonium Migration and Reduction of Halide Migration," *J. Phys. Chem. Lett.*, vol. 11, no. 17, pp. 7127–7132, Sep. 2020, doi: 10.1021/acs.jpclett.0c01822.

[38] S. Pont *et al.*, "Tuning CH 3 NH 3 Pb(I 1−x Br x) 3 perovskite oxygen stability in thin films and solar cells," *J. Mater. Chem. A*, vol. 5, no. 20, pp. 9553–9560, 2017, doi: 10.1039/C7TA00058H.

[39] D. Yan, M. Liu, Z. Li, and B. Hou, "Colloidal quantum dots and metal halide perovskite hybridization for solar cell stability and performance enhancement," *J. Mater. Chem. A*, vol. 9, no. 28, pp. 15522–15541, 2021, doi: 10.1039/D1TA02214H.

[40] S. Sidhik, C. Rosiles Pérez, M. A. Serrano Estrada, T. López-Luke, A. Torres, and E. De la Rosa, "Improving the stability of perovskite solar cells under harsh environmental conditions," *Sol. Energy*, vol. 202, no. February, pp. 438–445, May 2020, doi: 10.1016/j.solener.2020.03.034.

[41] Y. Yang and W. Wang, "Effects of incorporating PbS quantum dots in perovskite solar cells based on CH3NH3PbI3," *J. Power Sources*, vol. 293, pp. 577–584, Oct. 2015, doi: 10.1016/j.jpowsour.2015.05.081.

[42] I. Ka, I. M. Asuo, R. Nechache, and F. Rosei, "Highly stable air processed perovskite solar cells by interfacial layer engineering," *Chem. Eng. J.*, vol. 423, p. 130334, Nov. 2021, doi: 10.1016/j.cej.2021.130334.

[43] R. Ma *et al.*, "Establishing Multifunctional Interface Layer of Perovskite Ligand Modified Lead Sulfide Quantum Dots for Improving the Performance and Stability of Perovskite Solar Cells," *Small*, vol. 16, no. 41, Oct. 2020, doi: 10.1002/smll.202002628.

[44] L. He, H. Su, Z. Li, H. Liu, and W. Shen, "Multiple Function Synchronous Optimization by PbS Quantum Dots for Highly Stable Planar Perovskite Solar Cells with Efficiency Exceeding 23%," *Adv. Funct. Mater.*, vol. 33, no. 17, Apr. 2023, doi: 10.1002/adfm.202213963.

[45] S.-S. Li *et al.*, "Intermixing-seeded growth for high-performance planar heterojunction perovskite solar cells assisted by precursor-capped nanoparticles," *Energy Environ. Sci.*, vol. 9, no. 4, pp. 1282–1289, 2016, doi: 10.1039/C5EE03229F.

[46] U. D. Menda *et al.*, "Thermal-Carrier-Escape Mitigation in a Quantum-Dot-In-Perovskite Intermediate Band Solar Cell via Bandgap Engineering," *ACS Photonics*, Sep. 2023, doi: 10.1021/acsphotonics.3c00738.

[47] G. Ribeiro *et al.*, "Sub-Bandgap Sensitization of Perovskite Semiconductors via Colloidal Quantum Dots Incorporation," *Nanomaterials*, vol. 13, no. 17, p. 2447, Aug. 2023, doi: 10.3390/nano13172447.

[48] M. F. Mohamad Noh *et al.*, "High-humidity processed perovskite solar cells," *J. Mater. Chem. A*, vol. 8, no. 21, pp. 10481–10518, 2020, doi: 10.1039/D0TA01178A.

[49] H. Zhang *et al.*, "Understanding the Effect of Delay Time of Solvent Washing on the Performances of Perovskite Solar Cells," *ACS Omega*, vol. 2, no. 11, pp. 7666–7671, Nov. 2017, doi: 10.1021/acsomega.7b01026.

[50] L. Chao, Y. Xia, B. Li, G. Xing, Y. Chen, and W. Huang, "Room-Temperature Molten Salt for Facile

Fabrication of Efficient and Stable Perovskite Solar Cells in Ambient Air," *Chem*, vol. 5, no. 4, pp. 995–1006, 2019, doi: 10.1016/j.chempr.2019.02.025.

[51] U. D. Menda *et al.*, "High-performance wide bandgap perovskite solar cells fabricated in ambient high-humidity conditions," *Mater. Adv.*, vol. 2, no. 19, pp. 6344–6355, 2021, doi: 10.1039/D1MA00432H.

[52] Y. Tu *et al.*, "Slot-die coating fabrication of perovskite solar cells toward commercialization," *J. Alloys Compd.*, vol. 942, p. 169104, May 2023, doi: 10.1016/j.jallcom.2023.169104.

[53] M. M. Byranvand *et al.*, "One-Step Thermal Gradient- and Antisolvent-Free Crystallization of All-Inorganic Perovskites for Highly Efficient and Thermally Stable Solar Cells," *Adv. Sci.*, vol. 9, no. 23, Aug. 2022, doi: 10.1002/advs.202202441.

[54] H. Chen, "Two-Step Sequential Deposition of Organometal Halide Perovskite for Photovoltaic Application," *Adv. Funct. Mater.*, vol. 27, no. 8, p. 1605654, Feb. 2017, doi: 10.1002/adfm.201605654.

[55] G. Nasti *et al.*, "Pyridine Controlled Tin Perovskite Crystallization," *ACS Energy Lett.*, vol. 7, no. 10, pp. 3197–3203, Oct. 2022, doi: 10.1021/acsenergylett.2c01749.

[56] S. K. Yadavalli, M. Chen, M. Hu, Z. Dai, Y. Zhou, and N. P. Padture, "Electron-beam-induced cracking in organic-inorganic halide Perovskite thin films," *Scr. Mater.*, vol. 187, pp. 88–92, 2020, doi: 10.1016/j.scriptamat.2020.05.062.

[57] X. Zheng, B. Chen, C. Wu, and S. Priya, "Room temperature fabrication of CH3NH3PbBr3 by anti-solvent assisted crystallization approach for perovskite solar cells with fast response and small J-V hysteresis," *Nano Energy*, vol. 17, pp. 269–278, 2015, doi: 10.1016/j.nanoen.2015.08.023.

[58] N. K. Kumawat, N. Jain, A. Dey, K. L. Narasimhan, and D. Kabra, "Quantitative Correlation of Perovskite Film Morphology to Light Emitting Diodes Efficiency Parameters," *Adv. Funct. Mater.*, vol. 27, no. 3, p. 1603219, Jan. 2017, doi: 10.1002/adfm.201603219.

[59] C.-G. Wu, C.-H. Chiang, and S. H. Chang, "A perovskite cell with a record-high-V oc of 1.61 V based on solvent annealed CH 3 NH 3 PbBr 3 /ICBA active layer," *Nanoscale*, vol. 8, no. 7, pp. 4077–4085, 2016, doi: 10.1039/C5NR07739G.

[60] Y. Du *et al.*, "Precursor engineering for performance enhancement of hole-transport-layer-free carbon-based MAPbBr3 perovskite solar cells," *J. Alloys Compd.*, vol. 832, p. 154902, 2020, doi: 10.1016/j.jallcom.2020.154902.

[61] B. S. Swain, M. A. K. Sheikh, S. Singh, R. Abdur, D. Jeong, and J. Lee, "CH 3 NH 3 PbBr 3 nanocubes-array for solar cell application," *Mater. Sci. Semicond. Process.*, vol. 74, pp. 361–368, Feb. 2018, doi: 10.1016/j.mssp.2017.10.050.

[62] H. Shen, R. Nan, Z. Jian, and X. Li, "Defect step controlled growth of perovskite MAPbBr3 single crystal," *J. Mater. Sci.*, vol. 54, no. 17, pp. 11596–11603, 2019, doi: 10.1007/s10853-019-03710-6.

[63] S. Masi *et al.*, "Chemi-Structural Stabilization of Formamidinium Lead Iodide Perovskite by Using Embedded Quantum Dots," *ACS Energy Lett.*, vol. 5, no. 2, pp. 418–427, Feb. 2020, doi: 10.1021/acsenergylett.9b02450.

[64] A. Younis *et al.*, "Enhancing Resistive Switching Performance and Ambient Stability of Hybrid Perovskite Single Crystals via Embedding Colloidal Quantum Dots," *Adv. Funct. Mater.*, vol. 30, no. 31, Aug. 2020, doi: 10.1002/adfm.202002948.

[65] C. Fei and H. Wang, "Age-induced recrystallization in perovskite solar cells," *Org. Electron.*, vol. 68, pp. 143–150, May 2019, doi: 10.1016/j.orgel.2019.02.010.

[66] J. Han *et al.*, "Hybrid PbS Quantum-Dot-in-Perovskite for High-Efficiency Perovskite Solar Cell," *Small*, vol. 14, no. 31, p. 1801016, Aug. 2018, doi: 10.1002/smll.201801016.

[67] J. M. Lourenço. The NOVAthesis LATEX Template User's Manual. NOVA University Lisbon. 2021. url: https://github.com/joaomlourenco/novathesis_word/raw/master/novathesis_word-FINAL-EN.pdf.

APPENDIX

A DEVICE FABRICATION

A.1 Substrate Preparation

After being cut, the glasses are cleaned in an ultra-sound bath according to the following: Hellmanex (Sigma-Aldrich) solution (1% v/v) for 30 min; deionised water for 15 min; deionised water for 15 min; acetone (Laborspirit) for 15 min; and IPA (Isopropyl alcohol) (Laborspirit) for 15 min.

A.2 Compact Layer (c-TiO_2)

The first solution is prepared by mixing 180 µL of titanium (IV) isopropoxide (Sigma-Aldrich) with 1.25 mL of ethanol absolute (99.9 %, Carlo Erba). This solution is mixed until it turns whiteish. The second solution is prepared by mixing 18 µL of HCl (Hydrochloric acid fuming 37 %, Merck) with 1.25 mL of ethanol absolute. Then, the second solution is poured into the first one slowly.

A.3 Mesoporous Layer (m-TiO_2)

For the m-TiO2 layer, 375 mg of titania paste (Sigma-Aldrich) were weighed and dissolved in 2.5 mL of ethanol absolute.

A.4 One-Step Deposition Method of $MAPbBr_3$

To prepare the perovskite precursor solution (1.0 M), 550.500 mg of PbBr2 (Lead (II) bromide, Sigma-Aldrich) and 167.955 mg of MABr (Methylammonium bromide, Sigma-Aldrich) are weighed, mixed, and dissolved in 1.5 mL of DMF (N,N Dimethylformamide, 99.8%, Extra Dry, AcroSeal™, ACROS Organics, Thermo Fisher Scientific) and DMSO (Dimethyl sulfoxide, 99.7%, Extra Dry, AcroSeal™, Thermo Fisher Scientific) (9:1 v/v). For 0.6 M and 0.8 M solutions multiply the masses by 0.6 and 0.8, respectively.

For solutions with pyridine, 1.0 M MAPbBr3 is used. After dissolving the powders in the solvents, 75 µL of 4-tert-butylpyridine (95 %, ABCR GmbH & Co) is added.

The solutions are stirred at 65 °C for at least 4 h and filtered by a 22 µm filter before use.

A.5 Two-Step Deposition Method of $MAPbBr_3$

For 1:1 ratio solution, 330.300 mg of PbBr2 (0.6 M) and 100.773 mg of MABr (0.6 M) are weighed in separate vials, and dissolved in 1.5 mL of DMF and IPA, respectively. The solutions are stirred at 65 °C for at least 4 h and filtered by a 22 µm filter before use. For 0.8 M and 1.0 M solutions multiply the masses by 1.33 and 1.67, respectively.

Regarding 1:0.27 ratio solution, 500.100 mg of $PbBr_2$ (1.0M) and 45.348 mg of MABr (0.27M) are weighed in separate vials, and dissolved in 1.5 mL of DMF and IPA, respectively.

A.6 PbS-QDs Addition to Perovskite Precursor Solution

For the ligand exchange a MAPbBr3 solution (0.15M) in 2 mL of DMF is prepared and stirred for at least 4 h at 65 ℃. This perovskite solution will act as a core-shell for the dots. Afterwards, 75 µL, 150 µL, 300 µL, and 750 µL from a PbS QDs (1000 nm emission peak, in octane, Quantum Solution™) solution are poured into different vials and octane is added to make up 2 mL, to prepare QDs with concentrations of 0.5 mg/mL, 1.0 mg/mL, 2.0 mg/mL, and 5.0 mg/mL, respectively. After that, the QDs solution is slowly dropped into the shell solution and let to stir overnight. Subsequently, the dots are purified. On this step, the octane is removed. Then, it's added again and removed, three times. Consequently, 1.2 mL of toluene (Merck) is added and right after the solution is centrifuged (Neya 16 Remi) for 5 min at 10000 rpm. After being centrifuged, the excess solution is removed, and the dots dried in vacuum.

A.7 HTL

To prepare the Spiro-MeOTAD solution, 45 mg of spiro-MeOTAD (Sigma-Aldrich) is dissolved in 0.6 mL of chlorobenzene, 17.1 µL of 4-tert-butylpyridine, and in 10.5 µL of lithium salt (Bis (trifluoromethane) sulfonimide lithium salt,99.95% trace metals basis, Sigma-Aldrich).

B CHARACTERISATION

B.1 SEM

Top view and cross-sectional images were obtained by scanning electron microscopy (SEM) (Hitachi Regulus 8220 and a Carl Zeiss Auriga crossbeam (SEM-FIB), respectively).

B.2 XRD

The films' structural characterisation was done by X-ray diffraction(XRD) using a PANalytical Xpert PRO MRD diffractometer, being the X-rays' source Cu K-alpha ($\lambda = 1.540598$ Å).

B.3 PL

Steady state photoluminescence (PL) of synthesised films was obtained using a Perkin Elmer LS55 with excitation at 300 nm.

B.4 UV-Vis Spectrophotometry

Films' reflectance and total transmittance to obtain their ultraviolet-visible (UV-Vis) absorbance spectrum was obtained by using Shimadzu UV-3101PC spectrophotometer's ISR-260 Integrating Sphere (240 nm to 800 nm wavelength range).

B.5 Profilometer

MAPbBr3 films' thickness was measured using XP-Plus Stylus Profiler (Ambios XP-Plus 200 Stylus) at a speed of 0.1 mm/s with an applied force of 1 mg.

B.6 Opto-Electronical Characterisation

Devices' J-V curves were obtained using Newport's Oriel® VeraSol (VeraSol LSH-7520) solar simulator by reverse scan under AM 1.5 G illumination conditions (1000 W/m2).

C STRUCTURAL AND OPTICAL CHARACTERISATION

This section presents structural and the optical characterisation of the synthesised MAPbBr3 films, discussed in the section Results and Discussion.

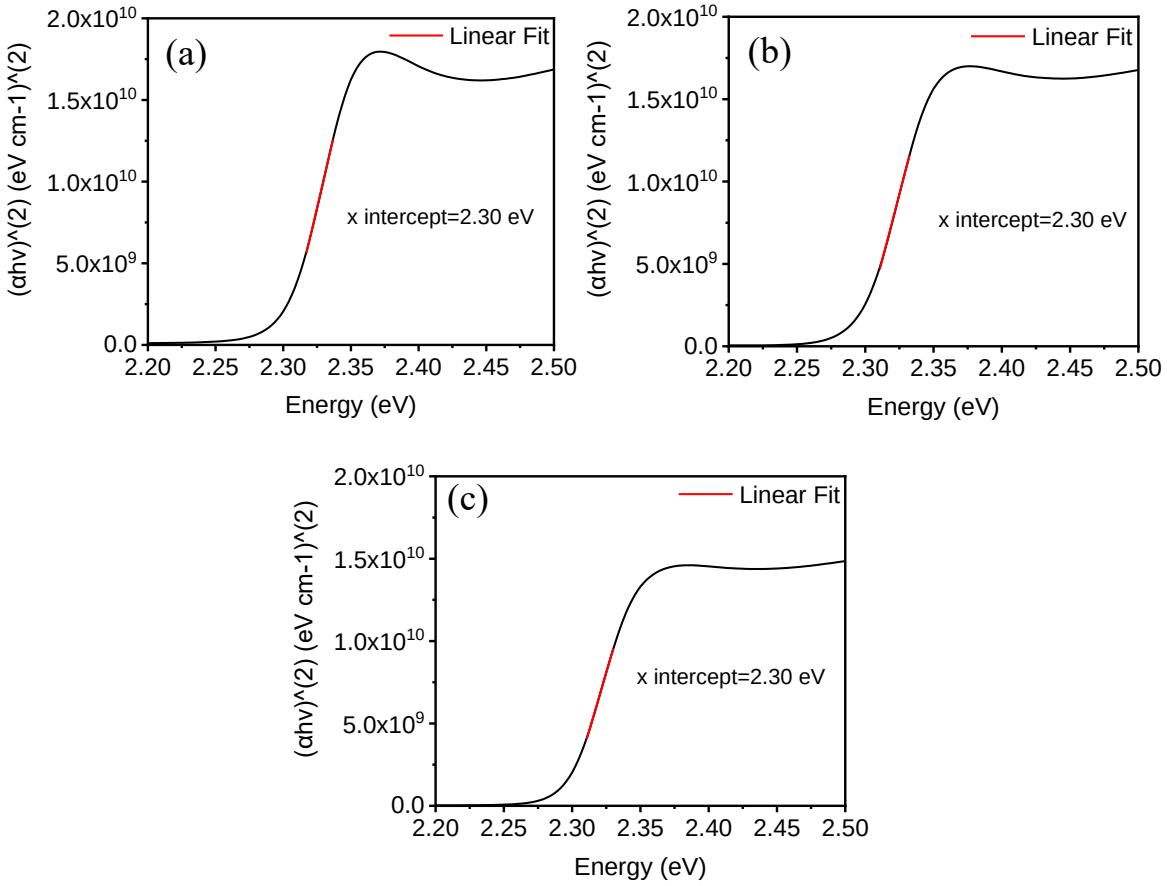

Figure 22. Tauc plot of one-step $MAPbBr_3$ films synthesised with 0.6 M (a), 0.8 M (b), and 1.0 M (b) precursor solutions, respectively.

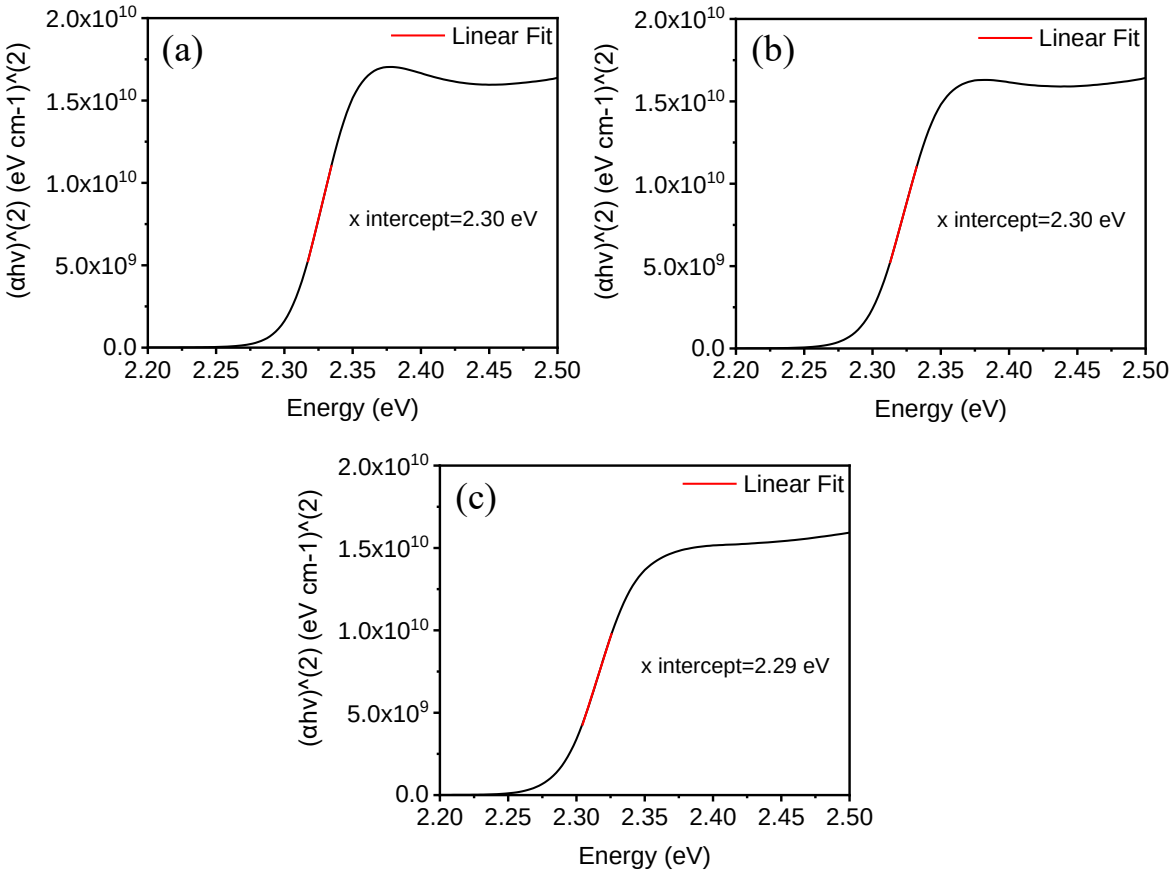

Figure 23. Tauc plot of $MAPbBr_3$ films synthesised via one-step deposition method using DMF/DMSO 1:0 (a), DMF/DMSO 9:1 (b) and DMF/DMSO 7:3 (c) ratios for the precursor solutions.

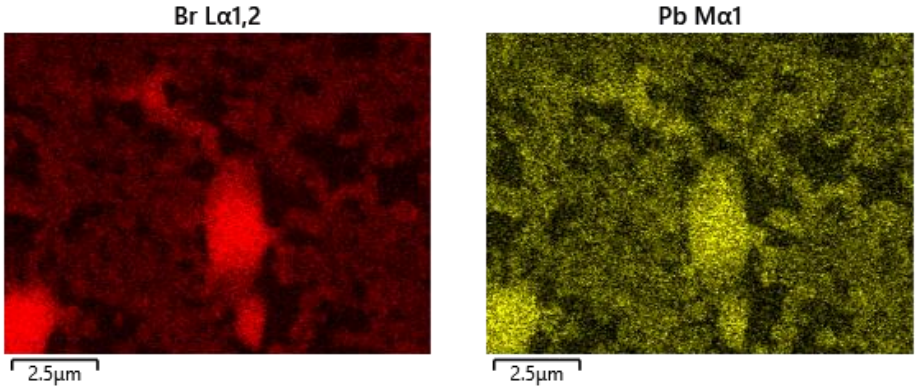

Figure 24. EDX mapping of $MAPbBr_3$ two-step films synthesised on a 1:1 ratio.

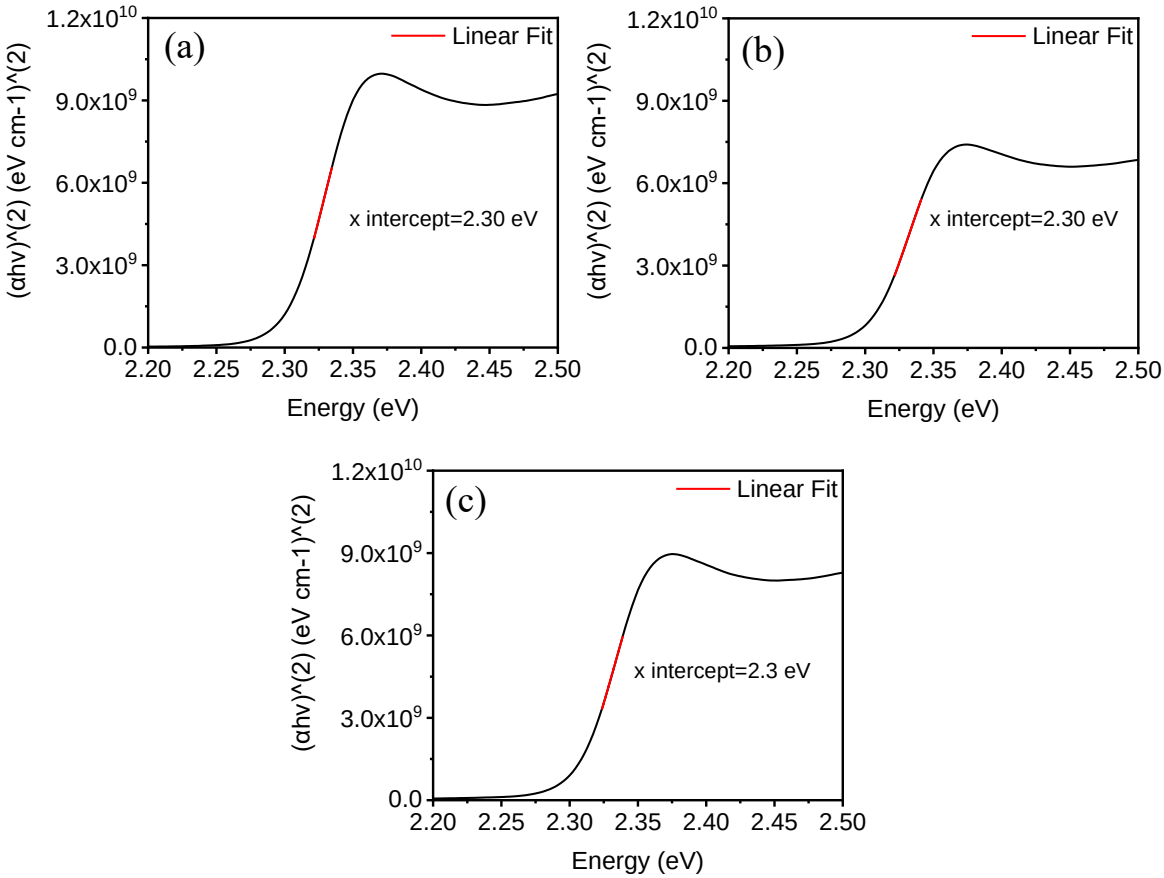

Figure 25. Tauc plot of two-step $MAPbBr_3$ films synthesised with 0.6 M (a), 0.8 M (b), and 1.0 M (c) precursor solutions, respectively.

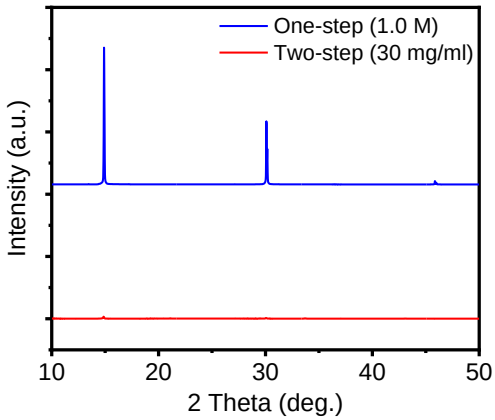

Figure 26. XRD of $MAPbBr_3$ films synthesised via one-step (1.0 M) and two-step (1:0.27) deposition methods.

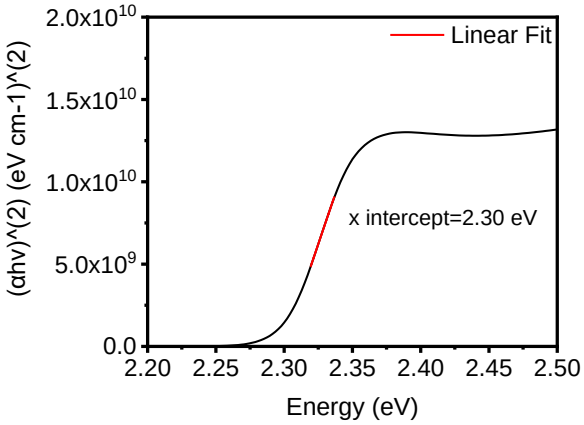

Figure 27. Tauc plot of the $MAPbBr_3$ film synthesised with pyridine.

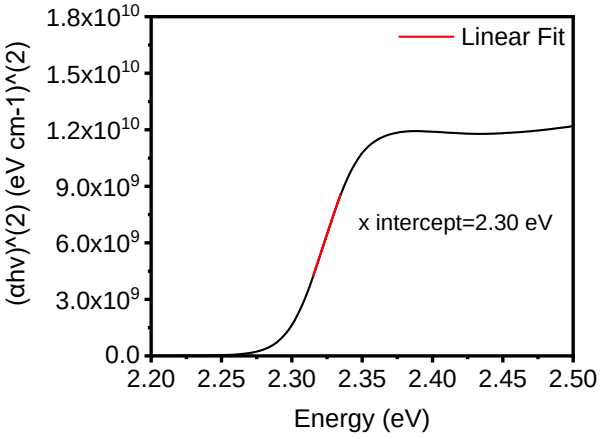

Figure 28. Tauc plot of $MAPbBr_3$ films synthesised with the inclusion of 0.05 mg/mL PbS QDs.

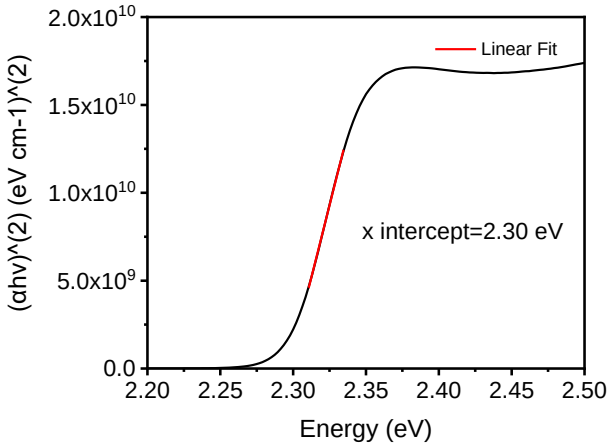

Figure 29 Tauc plot of $MAPbBr_3$ films synthesised with the inclusion of5.00 mg/mL PbS QDs.

D OPTOELECTRONIC CHARACTERISATION

This section presents the optoelectronic characterisation of the synthesised $MAPbBr_3$ devices, discussed in the section Results and Discussion.

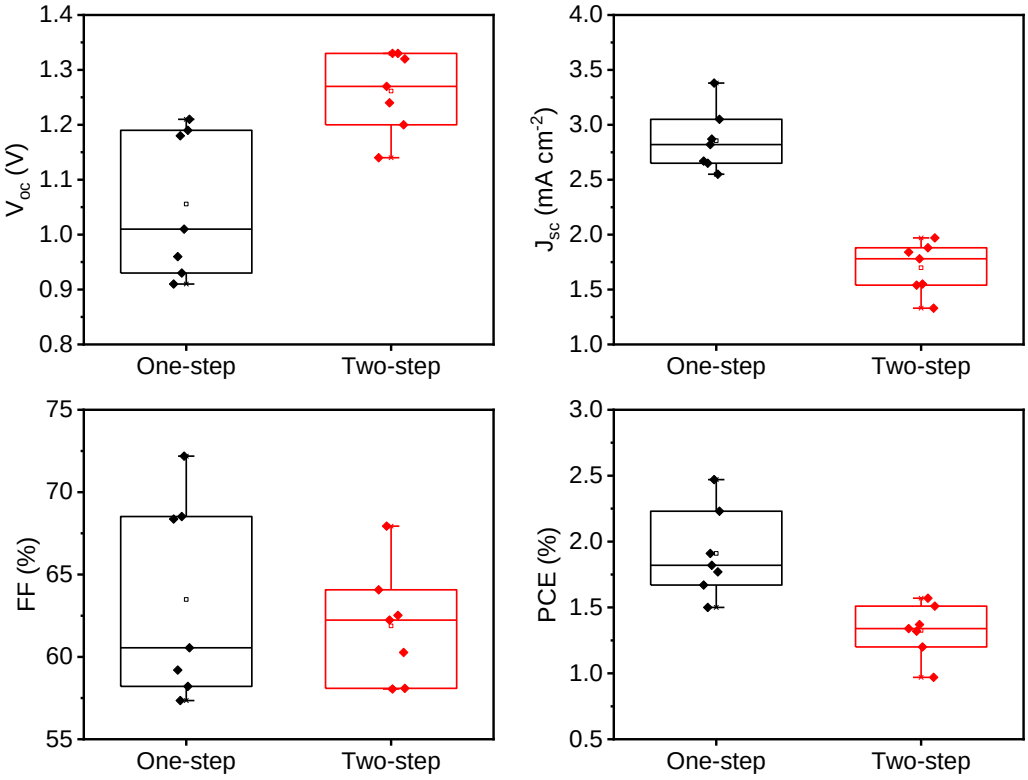

Figure 30 Box charts of the photovoltaic parameters obtained at reverse scan of $MAPbBr_3$ devices fabricated via one-step (1.0 M) and two-step (1:0.27).

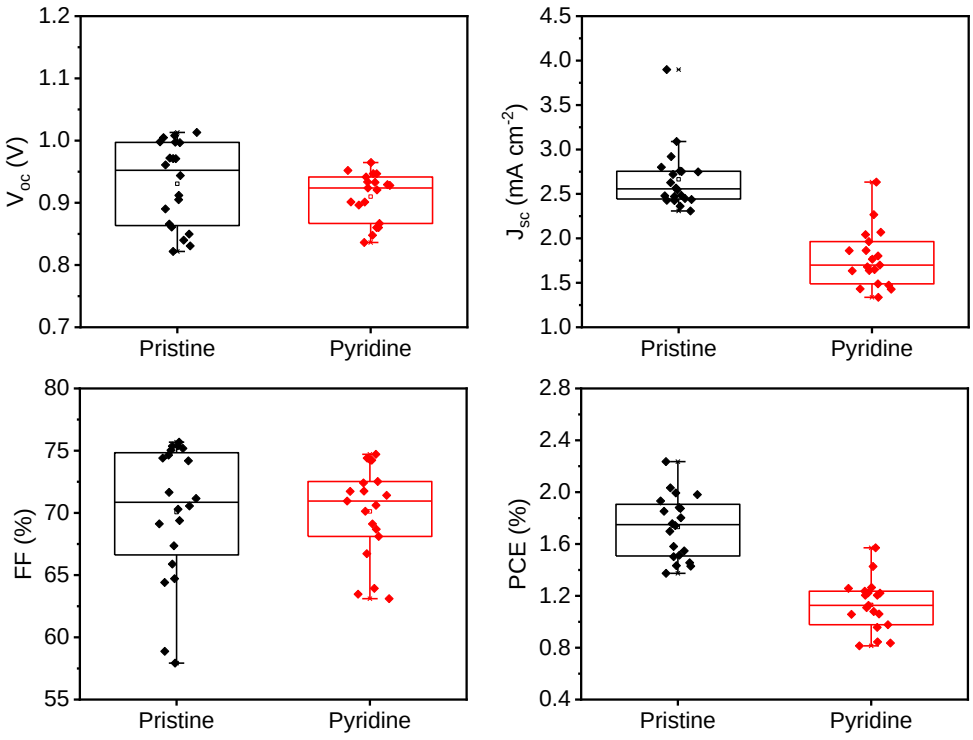

Figure 31 Box charts of the photovoltaic parameters obtained at reverse scan of $MAPbBr_3$ devices fabricated via one-step with and without pyridine addition in ambient air.

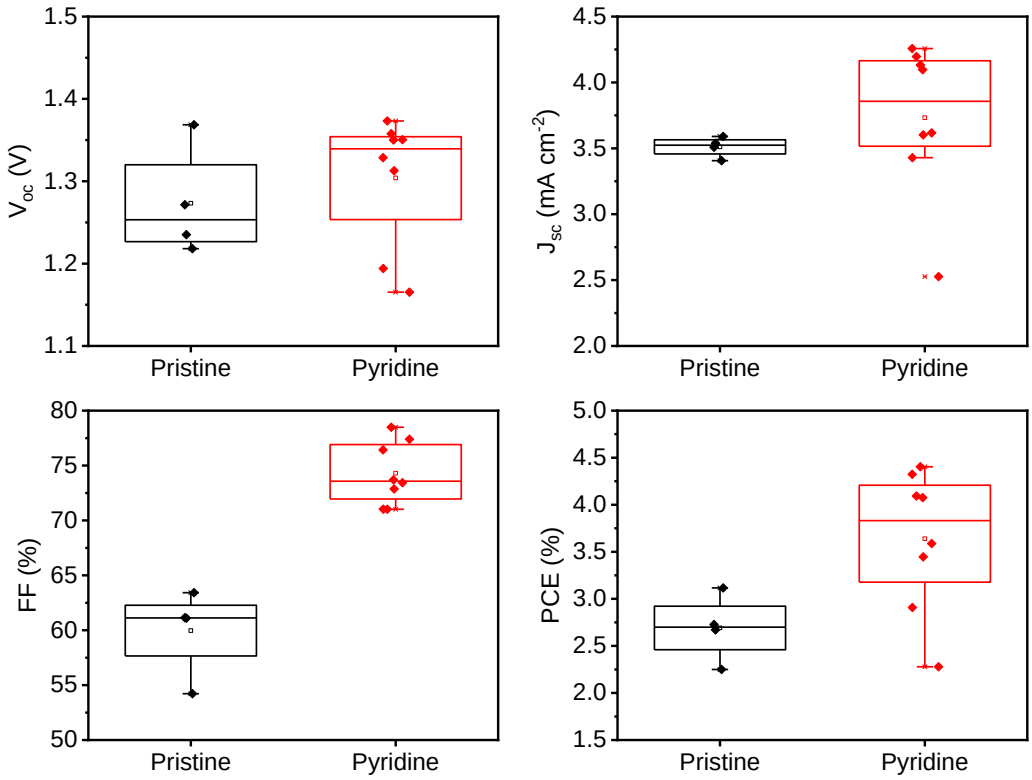

Figure 32 Box charts of the photovoltaic parameters obtained at reverse scan of $MAPbBr_3$ devices fabricated via one-step with and without pyridine addition inside the GB.

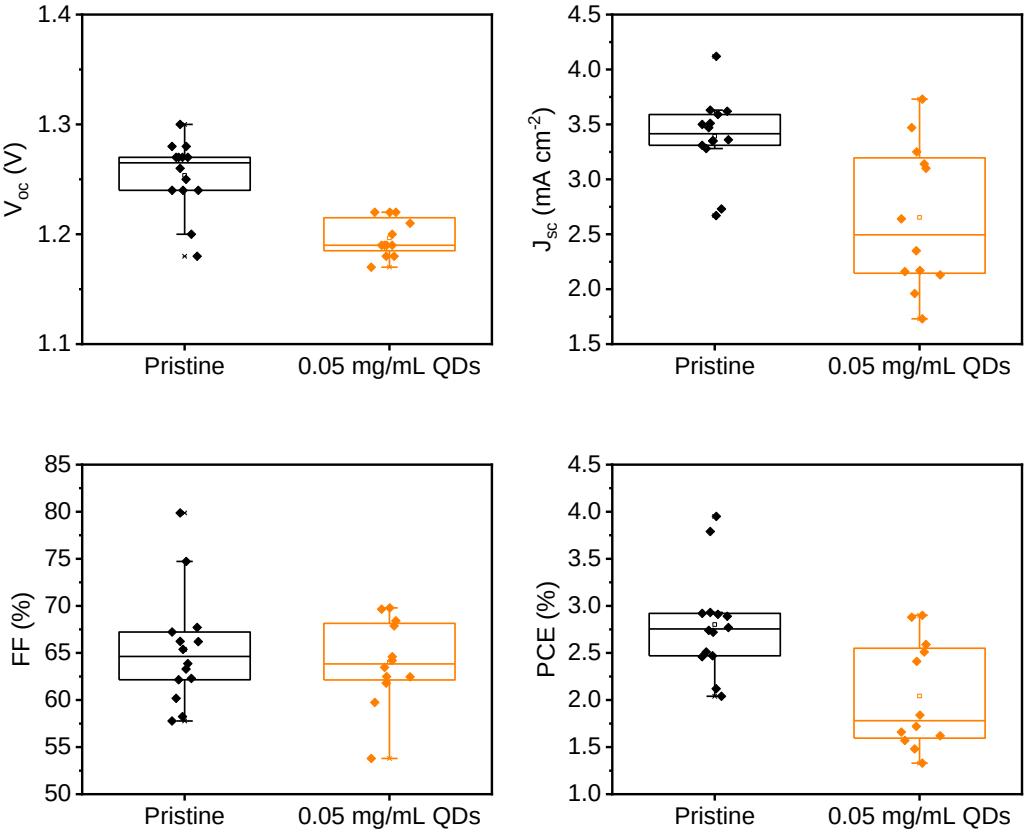

Figure 33 Box charts of the photovoltaic parameters obtained at reverse scan of $MAPbBr_3$ devices fabricated via one-step with (black) and without the inclusion of0.05 mg/mL PbS QDs (orange).

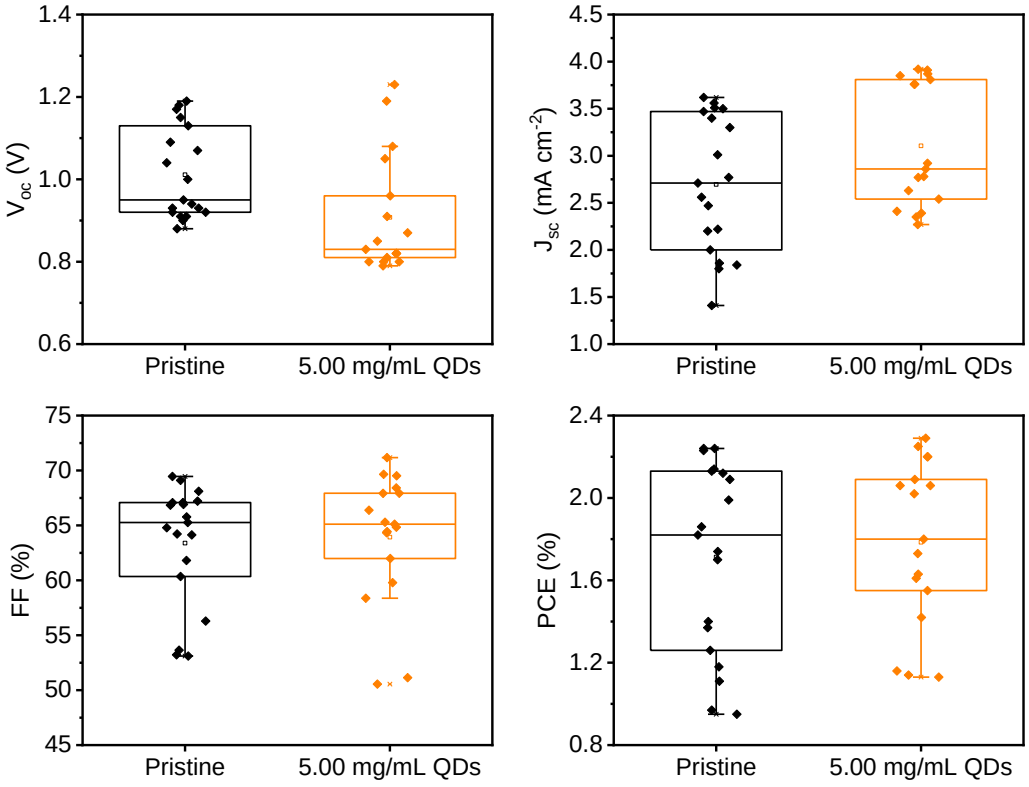

Figure 34 Box charts of the photovoltaic parameters obtained at reverse scan of $MAPbBr_3$ devices fabricated via one-step with and without the inclusion of 5.00 mg/mL PbS QDs.

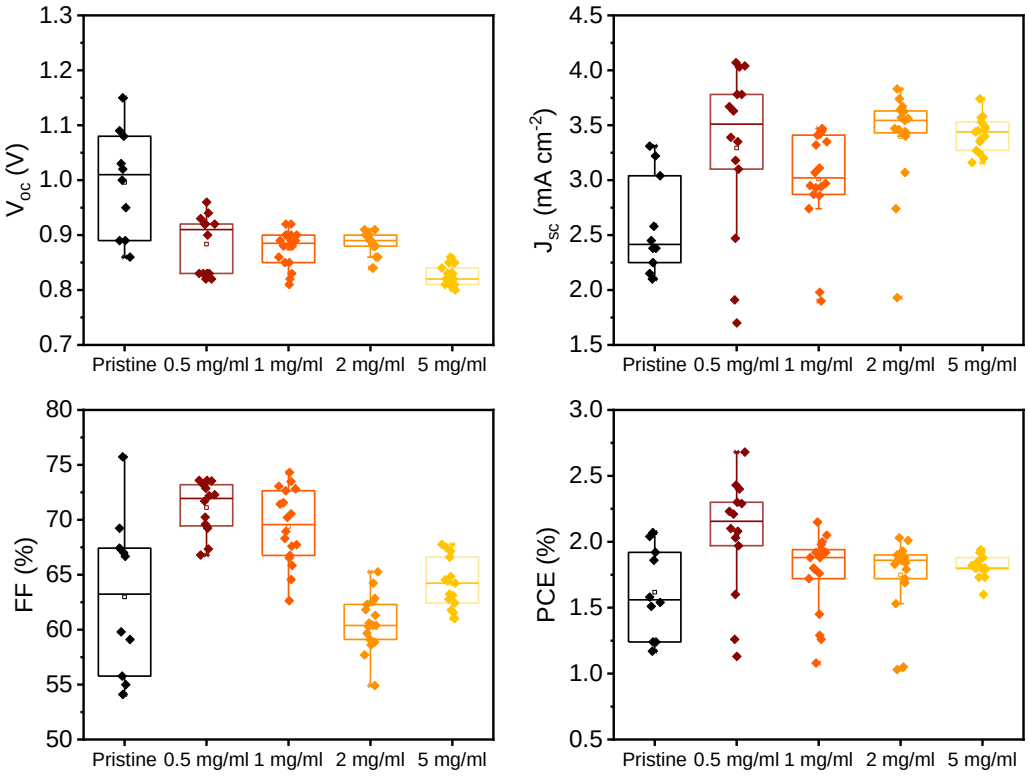

Figure 35 Box charts of the photovoltaic parameters obtained at reverse scan of $MAPbBr_3$ devices fabricated via one-step with and without 0.50 mg/mL, 1.00 mg/mL, 2.00 mg/mL, and 5.00 mg/mL PbS QDs.